ALL-LINEAR PHASE RETRIEVAL OF OPTICAL FREQUENCY COMBS VIA ELECTRIC FIELD CROSS-CORRELATION

A Thesis

Submitted to the Faculty

of

Purdue University

by

Ziyun Kong

In Partial Fulfillment of the

Requirements for the Degree

of

Master of Science in Electrical and Computer Engineering

May 2017

Purdue University

West Lafayette, Indiana

THE PURDUE UNIVERSITY GRADUATE SCHOOL
STATEMENT OF THESIS APPROVAL

Dr. Andrew M. Weiner, Chair

School of Electrical and Computer Engineering

Dr. Zubin Jacob

School of Electrical and Computer Engineering

Dr. Tongcang Li

Department of Physics and Astronomy

Approved by:

Dr. Venkataramanan Balakrishnan

Head of the Departmental Graduate Program

ACKNOWLEDGMENTS

I would like to thank my advisor, Prof. Andrew M. Weiner for the research opportunities, support and guidance provided; Lab manager Dr. Daniel Leaird for his help in experimental skills and technical suggestions; Dr. Chengying Bao who had worked closely with me in the experiments for his mentorship and patience; And all fellow members of the Ultrafast Optics Lab for the advice and helpful discussions.

TABLE OF CONTENTS

Page

LIST OF TABLES

LIST OF FIGURES

Figure Page

ABBREVIATIONS

OFC	Optical Frequency Comb
EFXC	Electric Field Cross-correlation
AC	Auto-correlation
FWHM	Full Width at Half Maximum
OSA	Optical Spectrum Analyzer
CW	Continuous Wave
EO-comb	Electrooptic comb

ABSTRACT

Kong, Ziyun M.S.E.C.E, Purdue University, May 2017. All-linear Phase Retrieval of Optical Frequency Combs via Electric Field Cross-correlation. Major Professor: Andrew M. Weiner.

Since the invention of optical frequency combs(OFCs), full optical waveform characterization has always been an important topic in ultrafast optics. Traditional measurements either provide only partial information of the waveform(auto-correlation) or require high power and low duty cycle of the waveform for nonlinear effects (FROG and SPIDER). In this thesis, we introduce an all-linear method for the phase retrieval of optical frequency combs. Through the dual-comb electric field cross-correlation between the signal comb and a pre-characterized reference comb, the beat signal is captured by real time oscilloscope in milliseconds. Post digital signal processing could retrieve phase from the sampled signal. The stability and precision of this method are discussed and phase retrieval from different combs generated through microresonators is performed.

1. INTRODUCTION

Optical waveform characterization is always an important topic in ultrafast optics. While the common intensity autocorrelation only gives a partial information about the measured field, a measurement for the complex field $E(t)$ is needed for full characterization.

Conventional methods for ultrafast waveform reconstruction, such as frequency-resolved optical gating(FROG, [1]) and spectral phase interferometry for direct electric field reconstruction (SPIDER, [2]) are all capable of recovering phase profile of input pulse. But due to the nonlinearity involved, these methods are often applied to waveforms with high peak power and low duty cycle.

In this thesis we'll introduce an all-linear phase retrieval method via dual-comb electric field cross-correlation(EFXC) [3, 4], which greatly lowers the power limit for phase retrieval of optical frequency combs.

1.1 Optical Frequency Comb

Ultrashort laser pulse widths were brought into femtosecond regime in the 1980s [5]. And now, optical frequency combs based on ultrafast lasers have already been a fundamental instrument for many research fields [6], like optical frequency measurement, high speed asynchronous optical sampling(ASOPS), absolute distance measurement and so on [7, 8]. In recent years, optical frequency combs(OFC) and ultrastable lasers have made great contributions to precision spectroscopy [9]. Now a spectral purity transfer based on narrow line-width OFC has reached a precision of 10^{-18} [10].

The Nobel Prize in Physics 2005 was divided, one half awarded to Roy J. Glauber "for his contribution to the quantum theory of optical coherence", the other half jointly to John L. Hall and Theodor W. Hänsch "for their contributions to the devel-

opment of laser-based precision spectroscopy, including the optical frequency comb technique" [11].

The output of a frequency comb in time domain is a pulse train with a regular period and a well-defined relative phase from pulse to pulse. In frequency domain, as shown in Fig 1.1, it is composed of multiple evenly spaced frequency components [12]:

$$f_N = N \times f_r + f_{ceo} \tag{1.1}$$

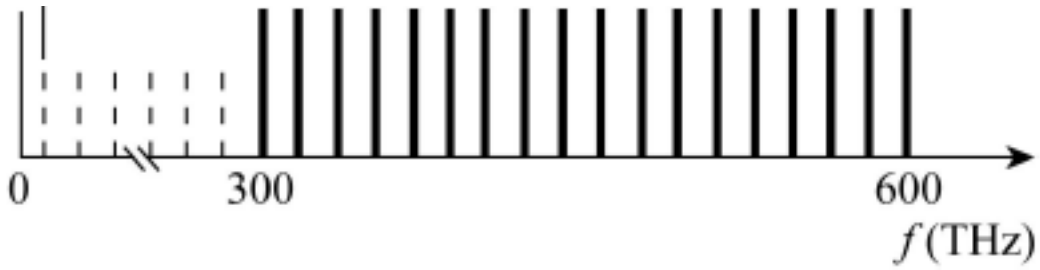

Fig. 1.1. Optical frequency comb(OFC) in frequency domain

Where f_r stands for the repetition rate of the laser and f_{ceo} is the carrier envelope offset frequency. The difference between group velocity and phase velocity within the cavity causes a carrier envelope offset. In the time domain it occurs as the relative phase difference between adjacent pulses, see Fig 1.2. In frequency domain it becomes a f_{ceo} signal [13]:

$$f_{ceo} = f_r \frac{\Delta\phi}{2\pi} \tag{1.2}$$

A mode-locked laser with both f_r and f_{ceo} stabilized could be considered as a stable frequency comb system and can be used as a frequency standard.

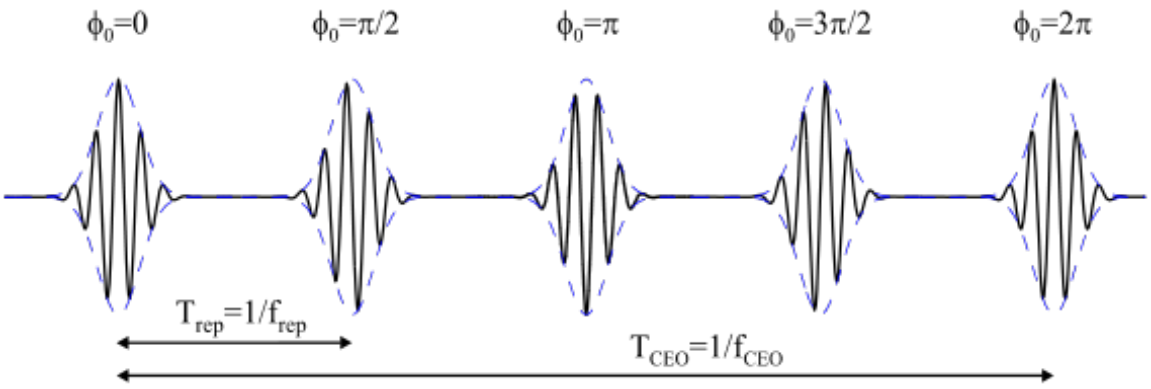

Fig. 1.2. Carrier envelope offset between pulses [14]

1.1.1 OFC generation from a Mode-locked laser

Due to its high efficiency and high output power, OFC based on a mode-locked laser is getting increasing attention [15, 16].Fig 1.3 shows a Yb: fiber ring laser with the highest rep rate (1 GHz) among fiber ring lasers so far.

It uses nonlinear polarization evolution (NPE) for passive mode-locking [18] and introduces a grating pair into the cavity so that the laser can work in the stretched pulse regime [19] with a close-to-zero net dispersion. Due to high rep rate, a high input power is needed, where they use four laser diodes to pump and acquired nearly 1W input on each side. The output of this laser is coupled into a tapered photonic-crystal fiber(PCF) for spectrum broadening. The broadened spectrum shown in Fig 1.4(b) right is octave-spanning. Then the output is coupled into an interferometer for $f - 2f$ beating to acquire the f_{ceo} signal, see schematic on Fig 1.4(a). The 1200nm part goes through the dichroic mirror and the 600nm part was reflected. Thus the second harmonic of 1200nm beats with the 600nm part and shows the f_{ceo} signal.

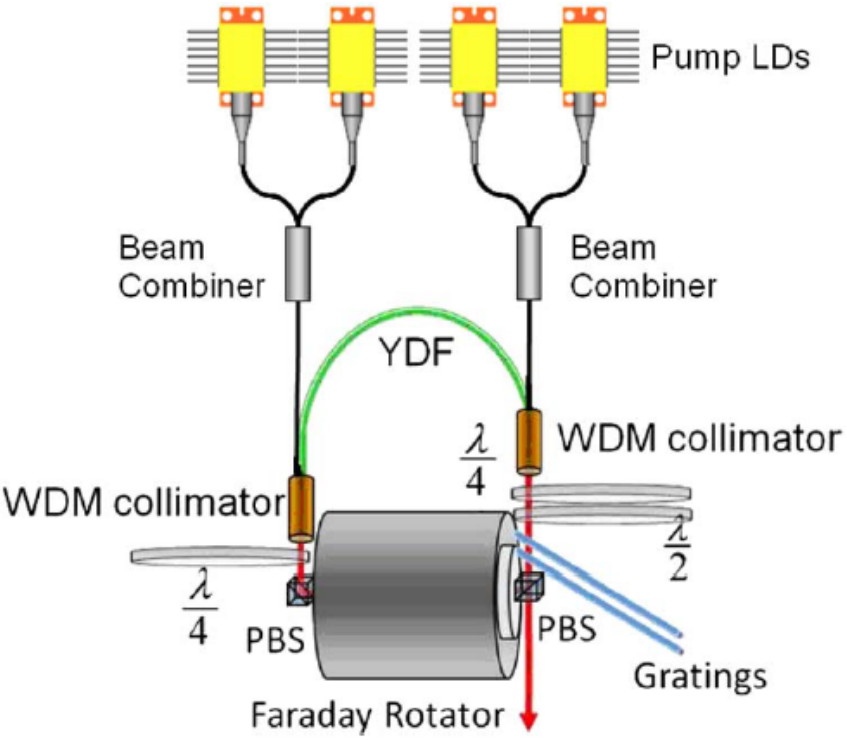

Fig. 1.3. Setup for 1 GHz Ytterbium-doped fiber ring laser. LD, laser diode; YDF, Ytterbium-doped fiber; WDM, wavelength division multiplexing; $\frac{\lambda}{2}$,$\frac{\lambda}{4}$, half/quarter-wave plate [17]

The f_{ceo} signal is acquired by a SHG of an original comb line with frequency

$$f_n = nf_r + f_{ceo} \tag{1.3}$$

After SHG, the comb line has its frequency doubled to

$$2f_n = 2nf_r + 2f_{ceo} \tag{1.4}$$

And meanwhile, a comb line formed by spectrum broadening has a frequency of

$$f_{2n} = 2nf_r + f_{ceo} \tag{1.5}$$

Thus results in a beating signal of

$$\Delta f = 2f_n - f_{2n} = f_{ceo} \tag{1.6}$$

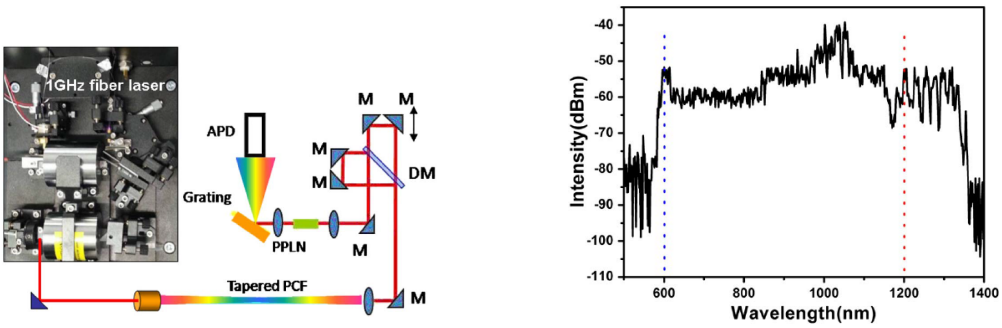

(a) (b)

Fig. 1.4. (a) Setup of the supercontinuum generation through tapered PCF and $f-2f$ beating. DM, dichronic mirror; APD, avalanche photodiode; PCF, photonic-crystal fiber; PPLN, periodically poled lithium niobate($LiNbO_3$). (b) Supercontinuum spectrum generated from the tapered PCF. The blue and red dotted lines show the octave-spanning spectrum from 600nm to 1200nm. [17]

The $f-2f$ detection of f_{ceo} provides a precise active stabilization of f_{ceo} if the detected signal is then compared with a RF frequency standard to generate an error signal. The error signal is fed back to the pump laser in order to finally stabilize f_{ceo} [20]. The frequency comb with both f_r and f_{ceo} well defined now serves as a precise optical frequency standard.

Another approach to generate OFCs with well defined f_{ceo} is through difference-frequency generation(DFG) [21]. In this method, a comb with more than octave-spanning spectrum is generated for a DFG comb with the same center frequency. The DFG signal between highest and lowest frequency components cancels the f_{ceo}, resulting in an offset-free comb:

$$\begin{aligned} f_{high} &= 2nf_r + f_{ceo} \\ f_{low} &= nf_r + f_{ceo} \\ f_{DFG} &= nf_r \end{aligned} \tag{1.7}$$

If carefully characterize the wavelength of the broadened comb, the DFG signal could also be centered at the pump frequency. This method is now applied to combs with repetition rate from tens of MHz to 1 GHz [22, 23].

One of the advantages of a mode-locked laser based OFC is that the laser is self-referenced, which means it could be easily locked to an atomic clock or similar RF standards to provide an absolute, wide-band frequency standard with high stability. Its high output power also makes it good for super-continuum generation, which leads to many applications including Astro-Comb [24].

But the f_r of this laser is dominantly limited by the ring cavity structure, where this limitation leads to a relatively small mode spacing(f_r) incapable with many other applications. As seen in Fig 1.3, the cavity is mainly filled up with a Faraday rotator and Yb gain fiber. As these two are the real essentials for this cavity where one provides the gain and the other ensures the pulse goes around the cavity in a specific direction, the f_r of this cavity is already near its limit as 1 GHz.

1.1.2 Electro-optic comb

Efforts have been made for a simple and direct OFC generation without complicated instrumental process. And the outcome is electro-optic comb, EO comb for short, which is obtained through direct modulation of a CW laser.

The principle of EO comb is that strong sinusoidal phase modulation of a CW laser creates multiple sidebands, leading to generation of a frequency comb. As shown in Fig 1.5, CW light with a narrow spectrum emitted from the laser is converted to phase-modulated light with ultrawide optical sidebands in the frequency domain ($\sim$THz). In time domain we could see that its converted to repeatedly chirped light. After compression or further modulation we retrieve a directly modulated EO comb.

Phase modulation of a CW laser can be achieved through electro-optic modulators based on Pockels cells, namely phase modulators(PM). Within a Pockels cell, the

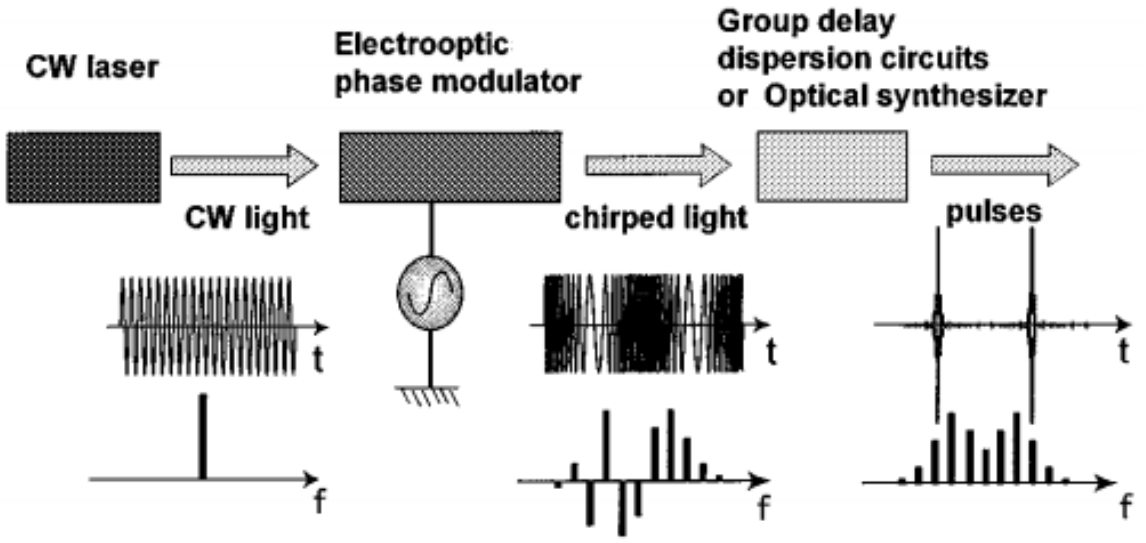

Fig. 1.5. Basic setup of comb generation through direct electro-optic modulation of CW laser [25]

birefringence of the nonlinear crystal is proportional to the input electric field, which is known as the Pockels effect or the linear electro-optic effect [26].

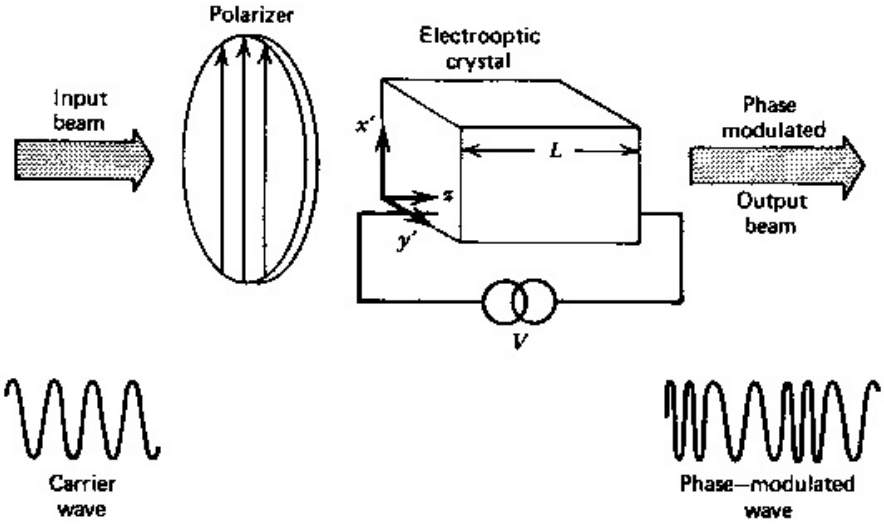

Fig. 1.6. Basic scheme of a phase modulator. Figure adapted from [26]

As shown in Fig 1.6, the input of a phase modulator is polarized parallel to one of the birefringent axes of the electrooptic crystal to avoid possible rotation of polarization. Thus the crystal now acts as a voltage-controlled wave-plate. A driving voltage of frequency ω will then apply a time-dependent phase $\Delta\phi \sin(\Omega t)$ to the input field $Ae^{i\omega t}$, resulting in output of

$$Ae^{i\omega t + i\Delta\phi \sin(\Omega t)} \tag{1.8}$$

Taking the assumption that $\Delta\phi \ll 1$, the output is approximated to

$$\begin{aligned} Ae^{i\omega t}(1 + i\Delta\phi \sin(\Omega t)) &= Ae^{i\omega t}\left(1 + \frac{\Delta\phi}{2}(e^{i\Omega t} - e^{-i\Omega t})\right) \\ &= A\left(e^{i\omega t} + \frac{\Delta\phi}{2}e^{i(\omega+\Omega)t} - \frac{\Delta\phi}{2}e^{i(\omega-\Omega)t}\right) \end{aligned} \tag{1.9}$$

by taking only the first term in Taylor expansion. This gives the sideband at $\omega + \Omega$ and $\omega - \Omega$. Deriving the whole series gives the amplitude of any sideband.

Here $\Delta\phi$ is known as the modulation depth of the PM. The Carson bandwidth rule for phase modulation gives the bandwidth of the generated sidebands [25]:

$$\Delta\nu = 2f\Delta\phi \tag{1.10}$$

Example specifications of a commercial lithium niobate($LiNbO_3$) phase modulator is listed in table 1.1. If we take 1 W as the maximum RF input power, a single PM can generate sidebands of bandwidth $\sim$ 200 GHz at a typical modulation frequency of 10 GHz ($\sim$ 20 lines). For a compressed pulse with bandwidth $\Delta\nu$, the pulse width τ is given by

$$\tau \approx \frac{0.7}{\Delta\nu} \tag{1.11}$$

Similarly for the amplitude modulation, where the modulation term is not on the exponential, only two sidebands at $\omega + \Omega$ and $\omega - \Omega$ are acquired:

$$Ae^{i\omega t}(1 + \Delta\phi \sin(\Omega t)) = Ae^{i\omega t} + \frac{A\Delta\phi}{2i}\left(e^{i(\omega+\Omega)t} - e^{i(\omega-\Omega)t}\right) \tag{1.12}$$

Advantages of this technique include the ability to create large mode spacing combs with stable but tunable optical center frequencies given by the source laser and

Table 1.1.
Specification of phase modulator - Avanex IM10-P

Operating Wavelength	C+L-Band
Insertion Loss	2.5 dB
RF V_π(1 kHz)	3.5 V
RF V_π(10 GHz)	5 V

convenient tuning of the repetition rate given by modulation frequency. Combined with multiple stage modulation, one can achieve broadly tunable frequency combs. Fig 1.7 shows an EO comb with broadly tunable line spacing ranging from 6 GHz to 18 GHz. A comb with large mode spacing can also be combined with line by line pulse shaping to help with arbitrary waveform generation [27].

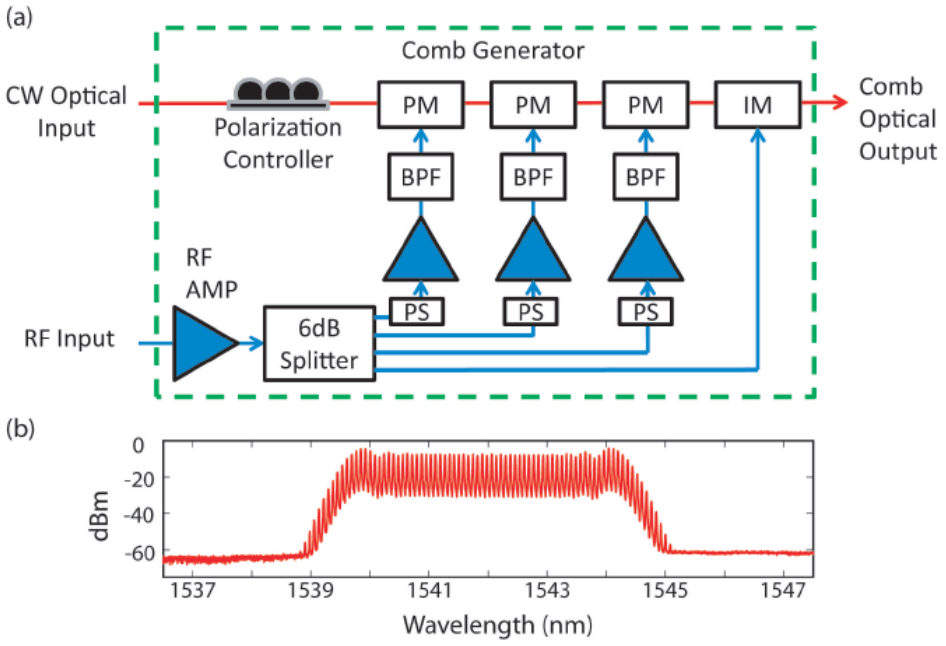

Fig. 1.7. (a) Layout of a broadly(6-18 GHz) tunable EO-comb. PM, phase modulator, IM,intensity modulator. (b) Example of output spectrum at $f_r = 10$ GHz [28]

.

1.1.3 Comb Generation through Microring Resonators

The methods for comb generation mentioned above provide frequency combs with repetition rate from several tens of MHz to $\sim$ 20 GHz. But still, optical frequency combs with even higher f_r are in great demand. Since 2007, frequency combs generated via Kerr effect in a microresonator with high quality factor(Q) have drawn people's attention for its compactness and potential for high repetition rate [29]. The comb generation is based on four-wave mixing (FWM). Two pump photons are annihilated to generate another pair of photons in this parametric frequency conversion [30],

$$2\omega_p = \omega_s + \omega_i \tag{1.13}$$

Where ω_p is the pump photon frequency; ω_s is the signal with higher frequency and ω_i is the idler with lower frequency. The conservation of energy restricts the signal and idler to be equidistant from the pump($\omega_s = \omega_p + \Omega$, $\omega_i = \omega_p - \Omega$). One can efficiently generate sidebands once ω_s and ω_i coincides with modes of microresonator. The total bandwidth is further increased through both degenerate and non-degenerate FWM, resulting in a broadband, equally-spaced optical spectrum, as shown in Fig 1.8.

The repetition rate of these combs ranges from several GHz to THz, which is far beyond what is achieved through mode-locked lasers. Octave Spanning spectrum from a sub-THz frequency comb is presented [31], and $f - 2f$ self-referenced microcomb is also realized [32].

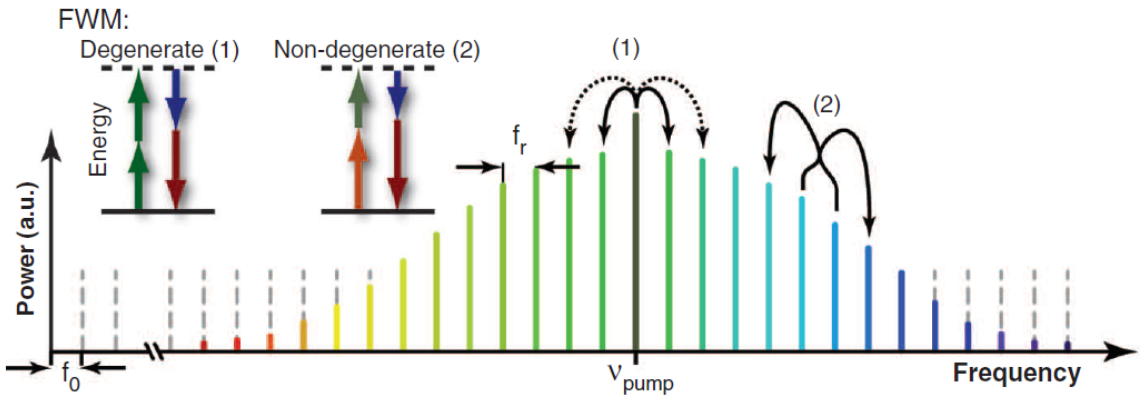

Fig. 1.8. Formation of frequency comb through FWM. (1)Degenerate FWM where two photons of the same frequency is converted(e.g. $2\omega_p = (\omega_p + \Omega) + (\omega_p - \Omega)$).(2) Non-degenerate FWM where two photons of different frequency is converted(e.g. $\omega_p + (\omega_p + \Omega) = (\omega_p - \Omega) + (\omega_p + 2\Omega)$). Figure adopted from [30]

1.2 Organization of Thesis

The remainder of this thesis is organized as follows. Section 2.0 will present the dual-comb electric field cross-correlation process and the physics involved. Section 3.0 will show the DSP method and algorithms used in phase retrieval process. In Section 4.0, Retrieved phases of different combs under different conditions are presented in comparison with phase from simulation or other techniques. And section 5.0 will briefly summarize the thesis.

2. ELECTRIC FIELD CROSS-CORRELATION

2.1 Mathematical Description of Phase Retrieval

Given two input fields with amplitude E_1, E_2, frequency ω_1, ω_2 and phase ϕ_1, ϕ_2, we could describe the fields as:

$$E_1 \cos(\omega_1 t + \phi_1), E_2 \cos(\omega_2 t + \phi_2) \tag{2.1}$$

Through coupling the two fields, we have a input field of

$$E = E_1 \cos(\omega_1 t + \phi_1) + E_2 \cos(\omega_2 t + \phi_2) \tag{2.2}$$

A photodetector(PD) measures the intensity of the field

$$\begin{aligned} I \propto & |E_1 \cos(\omega_1 t + \phi_1) + E_2 \cos(\omega_2 t + \phi_2)|^2 \\ = & E_1^2 \cos^2(\omega_1 t + \phi_1) + E_2^2 \cos^2(\omega_2 t + \phi_2) + 2E_1 E_2 \cos(\omega_1 t + \phi_1)\cos(\omega_2 t + \phi_2) \end{aligned} \tag{2.3}$$

For a slow detector, both $E_1^2 \cos^2(\omega_1 t + \phi_1)$ and $E_2^2 \cos^2(i\omega_2 t + \phi_2)$ are DC terms, thus

$$\begin{aligned} I \propto & 2E_1 E_2 \cos(\omega_1 t + \phi_1)\cos(\omega_2 t + \phi_2) \\ = & E_1 E_2 \{\cos[(\omega_1 - \omega_2)t + (\phi_1 - \phi_2)] + \cos[(\omega_1 + \omega_2)t + (\phi_1 + \phi_2)]\} \end{aligned} \tag{2.4}$$

Still, the term $\cos[(\omega_1 + \omega_2)t + (\phi_1 + \phi_2)]$ is DC for a slow detector, so the beat signal is

$$\begin{aligned} I_{\text{Beat}} \propto & E_1 E_2 \cos[(\omega_1 - \omega_2)t + (\phi_1 - \phi_2)] \\ \text{or } I_{\text{Beat}} \propto & E_1 E_2 e^{i[(\omega_1 - \omega_2)t + (\phi_1 - \phi_2)]} \end{aligned} \tag{2.5}$$

with frequency $\omega_{beat} = \omega_1 - \omega_2$. Here the phase of the beat signal $\phi_{beat} = \phi_1 - \phi_2$ is the phase difference between two input fields. If we characterize the input fields in a way that ϕ_2 is known to us (e.g. let $\phi_2 = 0$), then ϕ_1 can be reversely retrieved through:

$$\phi_1 = \phi_{beat} + \phi_2 \tag{2.6}$$

with ϕ_2 already known.

In our case both ω_1 and ω_2 are optical frequencies. If we carefully choose the frequency of input fields so that ω_{beat} is in radio frequency(RF) band, using a slow detector will only capture the signal at beat frequency $\omega_{beat} = \omega_2 - \omega_1$. Thus the phase of input optical field can be retrieved from a RF signal, whose phase is easy to get through Fourier analysis.

Now we extend equation 2.5 to the beat signal between two combs. Suppose two combs A and B are represented by Dirac comb in frequency domain as

$$\begin{aligned} &\sum_{N=N_0}^{N_1} \delta[f - (N \times f_A + f_{ceoA})] \\ &\sum_{M=M_0}^{M_1} \delta[f - (M \times f_B + f_{ceoB})] \end{aligned} \tag{2.7}$$

Let $f_{Aj} = j \times f_A + f_{ceoA}$ be the jth line in comb A and $f_{Bk} = k \times f_B + f_{ceoB}$ be the kth line in comb B. The field then is described as

$$\begin{aligned} &\sum_{j=N_0}^{N_1} A_j e^{2\pi i f_{Aj} t + i\phi_j} \\ &\sum_{k=M_0}^{M_1} B_k e^{2\pi i f_{Bk} t + i\phi_k} \end{aligned} \tag{2.8}$$

where A_j, ϕ_j are amplitude and phase for the jth line in comb A and B_k, ϕ_k are amplitude and phase for the kth line in comb B. The beat signal between these two combs that appears pairwise between lines is

$$\sum_{N_0 \le j \le N_1, M_0 \le k \le M_1}^{f_{Aj} > f_{Bk}} C_{jk} e^{2\pi i (f_{Aj} - f_{Bk})t + i(\phi_{Aj} - \phi_{Bk})} + \sum_{N_0 \le j \le N_1, M_0 \le k \le M_1}^{f_{Aj} < f_{Bk}} C_{jk} e^{2\pi i (f_{Bk} - f_{Aj})t + i(\phi_{Bk} - \phi_{Aj})} \tag{2.9}$$

Following assumptions are made for simplicity:

- Comb B is broader than comb A (i.e. $f_{2M_1} > f - 1N_1$ and $f_{2M_0} < f - 1N_0$)
- $f_B < f_A$ so that $f_A = nf_B + \Delta f_{rep}$ where n is an integer and Δf_{rep} is the least positive remainder between f_B and f_A.

- There exists a line s from comb B that $f_{Bs} < f_{AN_0}$ and the difference $f_{min} = f_{AN_0} - f_{Bs}$ is minimized.
- Comb B has a pre-characterized phase profile where $\phi_{Bk} = 0$ for all $M_0 \leq k \leq M_1$.

Then the beat signal can be represented by

$$\sum_{j=0}^{N_1-N_0} C_j e^{2\pi i(f_{min}+j\Delta f_{rep})t+i\phi_{Aj}} + \sum_{j=0}^{N_1-N_0} C_j e^{2\pi i(f_B-f_{min}-j\Delta f_{rep})t-i\phi_{Aj}} \tag{2.10}$$

which serves as a down-converted spectrum of comb A. Illustration of equation 2.10 will be discussed in sec. 2.2.

2.2 Experimental View

To help with better understanding of the notation, we name the comb with pre-characterized phase the *reference comb* with line spacing f_{ref}; and the comb with unknown phase the *signal comb* with line spacing f_{sig}. Then the frequency of lines from the signal comb are $N \times f_{sig} + f_{ceo1}$ and lines from the reference comb are $N \times f_{ref} + f_{ceo2}$, where N is an integer.

We assume that $f_{sig} = n \times f_{ref} + \Delta f_{rep}$, where n is an integer and Δf_{rep} is the least positive remainder between f_{sig} and f_{ref}. Here we call Δf_{rep} the rep-rate difference between the signal and reference comb.

Also we assume that the beating process described in Sec 2.1 begins at a frequency difference of f_{min}, namely the lines beating with each other are at least of f_{min} difference in frequency. If we care only the beating between lines and their closest neighbor, it would result in a down converted signal comb spectrum in RF band from 0 to f_{ref} with spacing Δf_{rep}, as the yellow lines shown in Fig 2.1. Since the remainder between f_{sig} and f_{ref} is Δf_{rep}, the next pair of lines beating would occur at a frequency difference of $f_{min} + \Delta f_{rep}$, and the next beat signal with frequency $f_{min} + 2\Delta f_{rep}$ etc.

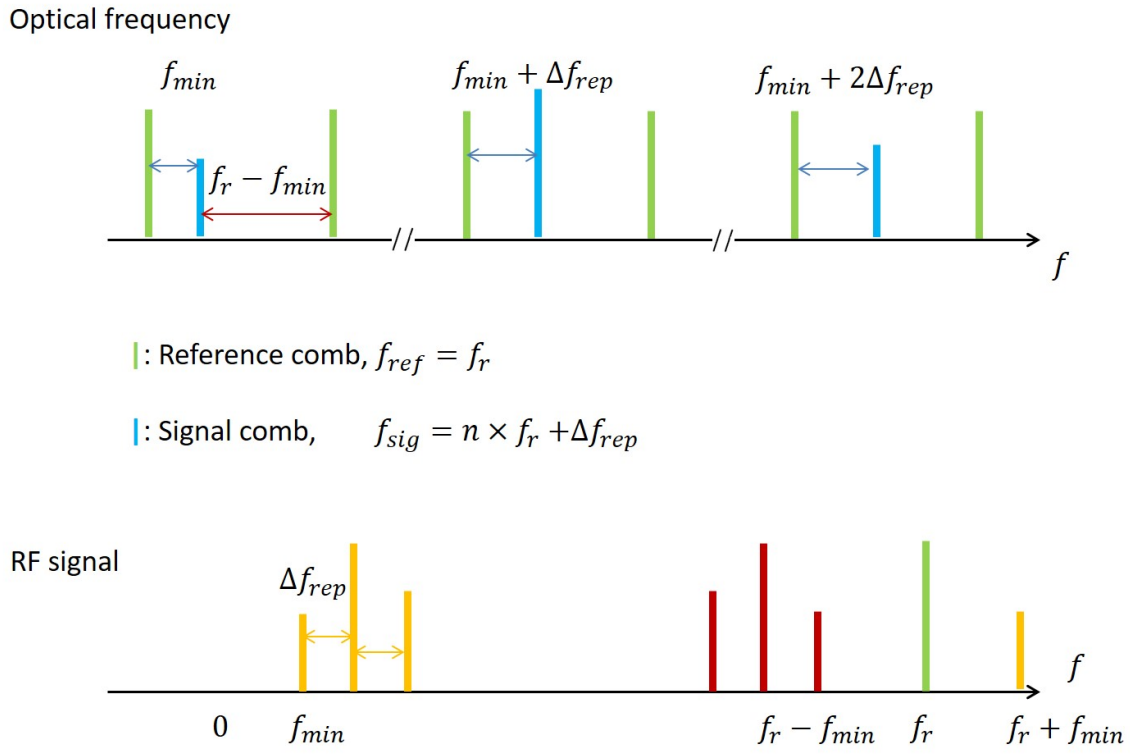

Fig. 2.1. Generation of down converted spectrum and mirror of signal comb

It's worth noting that for every signal line beating with its low frequency neighbor in reference comb with frequency difference f, it's also beating with its high frequency neighbor in reference comb with frequency difference $f_{ref} - f$. This generates a mirror of the RF spectrum traveling backwards from $f_{ref} - f_{min}$ with spacing $-\Delta f_{rep}$, as the red lines shown in Fig 2.1.

In order to perform a robust measurement, the down converted spectrum needs to be separated from its own mirror, meaning that the spectrum should stay within the range of either $0 - \frac{f_{ref}}{2}$ or $\frac{f_{ref}}{2} - f_{ref}$. Also if Δf_{rep} is set too large, the spectrum will spread beyond f_{ref} to beat with the next $n+1$th line instead of the nth, which would cause a wrapping of the RF spectrum, as shown in Fig 2.2.

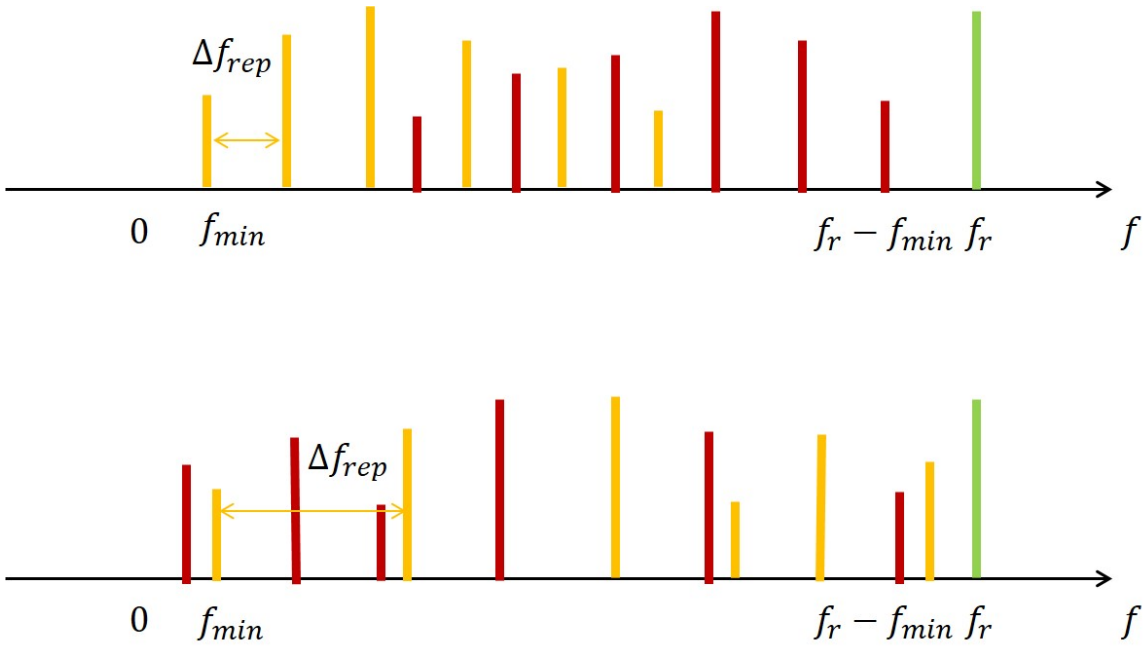

Fig. 2.2. Illustration of the overlapping(top) and wrapping(bottom) of the down converted spectrum.

Assume the numbers of total comblines resolved is N_{line}, for a simple scheme where the down converted spectrum stays within the range of $0 - \frac{f_{ref}}{2}$, the limitation above gives:

$$f_{min} + N_{line}\Delta f_{rep} < \frac{f_{ref}}{2} \tag{2.11}$$

for a distinguishable spectrum. In an experimental point of view, we can change f_{min} by tuning f_{ceo} of the reference comb and Δf_{rep} by tuning the repetition rate of the reference comb f_{ref} to meet the requirement above.

To further illustrate the beating process, a simulation through MATLAB is shown in Fig 2.3. In this simulation, we have a reference comb with rep-rate $f_{ref} = 250$ MHz to beat with a signal comb with rep-rate f_{sig} =200 GHz +1.5 MHz, which gives us a rep-rate difference Δf_{rep} =1.5 MHz. Both combs have a hyperbolic secant shaped spectrum and the signal comb has a strong pump line at 1550 nm. We also set the starting frequency $f_{min} = 20$ MHz.

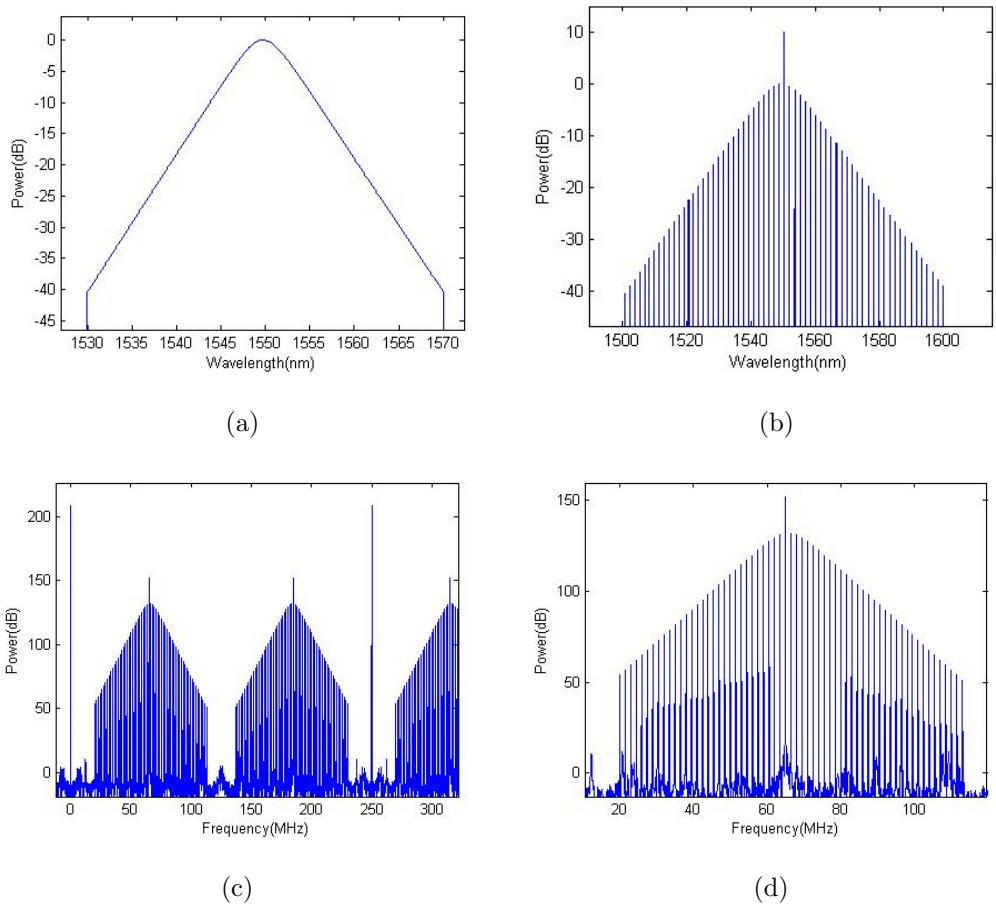

Fig. 2.3. Optical and RF spectrum acquired in simulation. (a) Spectrum of the reference comb. (b) Spectrum of the signal comb. (c) RF spectrum of the beating signal. (d) Fig (c) enlarged to show the down-converted spectrum of the signal comb in RF domain

2.3 Relation to conventional EFXC

Traditional electric field cross-correlation measures cross-correlational fringes with respect to the delay between signal and reference fields through a interferometer. The delay time is controlled by a mechanical translation stage. The fringes recorded by a slow detector can be written as a function of delay τ [27]:

$$\langle P_{out}(\tau)\rangle = \frac{1}{2}\{U_s + U_r + \int \{a_s(t)a_r^*(t-\tau)e^{j\omega_0\tau} + c.c.\}dt\} \tag{2.12}$$

Where U_s and U_r are DC terms introduced by signal and reference pulse energy and ω_0 is the carrier frequency for both signal and reference field. Then through Fourier analysis of the captured fringes one can recover the input field with knowledge of a well-defined reference field [33].

The reason for our method to be named after electric field cross-correlation is because that in traditional EFXC setup, the delay τ is controlled by a moving stage, while in our setup, the delay is introduced by the rep rate difference Δf_{rep} between the signal and reference comb, causing them to automatically sweep through each other in time without mechanical moving parts in setup, as shown in Fig 2.4.

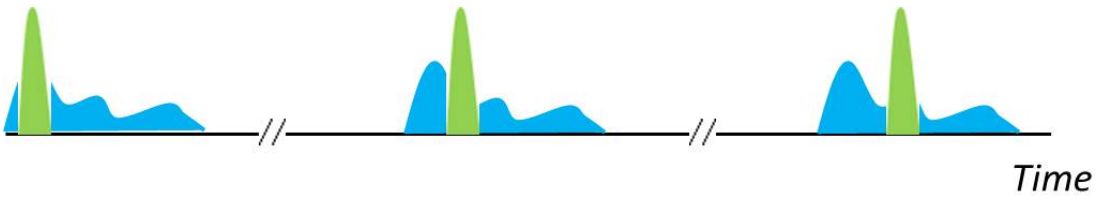

Fig. 2.4. Illustration of reference comb field(green) automatically sweeps through signal comb field(blue) in time due to Δf_{rep} difference in FSR.

3. DIGITAL SIGNAL PROCESSING

3.1 Discrete Fourier Transform

As from equation 2.5, the beat signal between signal and reference comb is given by:

$$I_{\text{Beat}} \propto E_1 E_2 e^{i[(\omega_1-\omega_2)t+(\phi_1-\phi_2)]} \tag{3.1}$$

If given the FSR difference between signal and reference comb Δf_{rep} and starting frequency f_{min}, the down-converted spectrum shown in Fig 2.1 can be described as

$$E(t) = \sum_{j=0}^{n} a_j e^{i(2\pi f_j t+\phi_j)} \tag{3.2}$$

where$f_j = f_{min} + j\Delta f_{rep}$, and a_k is the intensity of the beat signal, proportional to the product between corresponding lines ($E_1 E_2$).

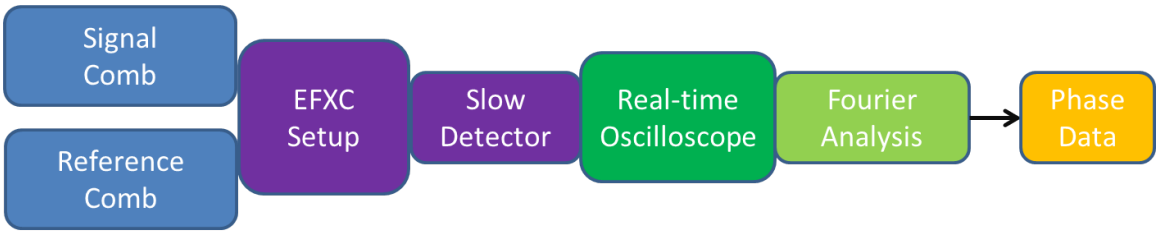

Fig. 3.1. Basic scheme for the phase retrieval experiment

Assuming reference comb has a pre-characterized phase of $\phi_{ref} = 0$, then ϕ_k would be the phase of corresponding lines of the signal comb. Fig 3.1 shows the basic scheme for this process.

The signal from photodetector is sampled by oscilloscope into a sequence of equally-spaced samples of finite length. Then the discrete Fourier transform(DFT)

converts the sequence into samples of its discrete-time Fourier transform(DTFT), giving the result in frequency domain.

The definition of DFT is given by

$$X_k \stackrel{\text{def}}{=} \sum_{n=0}^{N-1} x_n \cdot e^{-2\pi i k n/N}, k \in \mathbb{Z} \tag{3.3}$$

or in its trigonometric form

$$X_k \stackrel{\text{def}}{=} \sum_{n=0}^{N-1} x_n \cdot (\cos(-2\pi k \frac{n}{N}) + i \sin(-2\pi k \frac{n}{N})), k \in \mathbb{Z} \tag{3.4}$$

where N is the number of sampled points.

The input field $E(t)$ from equation 3.2 is sampled by a sample frequency f_s into a equally spaced sequence $E(n)$. The sequence after DFT is

$$\mathcal{F}(E(t)) = E(f_k) = \sum_{j=0}^{n} a_j e^{i\phi_j} \cdot \delta(f_j - f_k) \tag{3.5}$$

Note that here we already mapped the DFT sequence onto distinct frequency values $f_k = k\frac{f_s}{n}$. δ is the Dirac delta function, meaning that the input time series is converted into distinct complex values in frequency domain with argument ϕ_k.

3.2 Spectral Analysis

Considering the RF spectrum after DFT, it consists not only the beat signal, but also its mirror with respect to $\frac{f_r}{2}$ and the f_r component from the reference comb with lower line spacing. Thus equation 3.5 changes into

$$E(f_k) \propto \sum_{j=0}^{n} a_j \left[e^{i\phi_j} \cdot \delta(f_j - f_k) + e^{-i\phi_j} \cdot \delta(f_r - f_j - f_k)\right] + e^{i\phi_r} \cdot \delta(2\pi f_r - f_k) \tag{3.6}$$

where$f_k = f_{min} + k\Delta f_{rep}$, and a_k is the intensity of the beat signal. Fig 3.2 illustrates the RF spectrum after DFT.

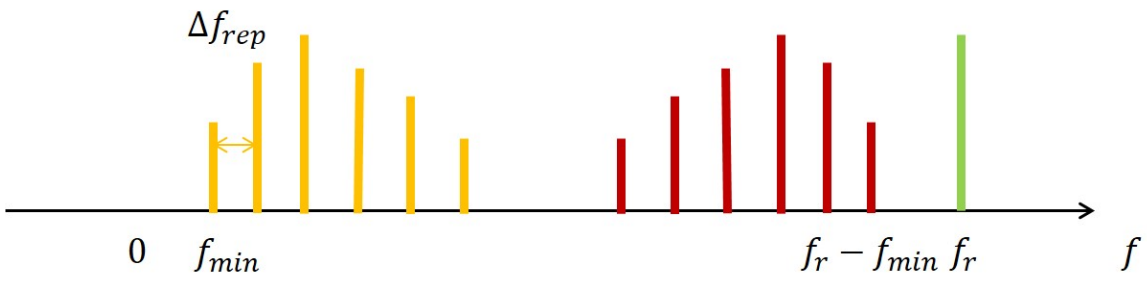

Fig. 3.2. Illustration of RF spectrum(with positive frequency) after DFT

3.2.1 Aliasing

Note that in Fig 3.2, the highest frequency component we are interested in is f_r. To minimize the possible aliasing effect, the Nyquist–Shannon sampling theorem [34] shows that for the sampling rate f_s of the oscilloscope,

$$f_s > 2f_r \tag{3.7}$$

A sampling rate lower than $2f_r$ would fail to resolve the f_r component, causing aliasing. In experimental point of view, oversampling of the signal would eliminate aliasing. And also for a time series sampled with sampling rate f_s, the Fourier transformed spectrum has a frequency range of $[-f_s/2, f_s/2]$ assuming using a $2N+1$ points FFT(fast Fourier transform) algorithm, causing the intensity noise to be spread out in frequency domain and increase signal-to-noise ratio(SNR). In practical setup we choose to use $f_s \approx 4f_r$.

3.2.2 Spectral leakage

For a N points series sampled by rate of f_s, the DFT spectrum has a frequency resolution of $\frac{f_s}{N}$, which means two adjacent points in frequency domain has a frequency

difference of $\frac{f_s}{N}$. Assuming the beat signal has a narrow linewidth compared to spectral resolution $\frac{f_s}{N}$, the spectrum can be seen as a Dirac comb in frequency:

$$\sum_{k=-\infty}^{\infty} \delta(f_{min} - k\Delta f_{rep}) \tag{3.8}$$

where Δf_{rep} is the period in frequency. For a DFT sequence of finite length N, DFT assumes that its input sequence is a N-periodic sequence in time. Thus a rectangular window of length N is applied to the original sequence. And we know that

$$\mathcal{F}(f(n) \cdot g(n)) = \mathcal{F}(f(n)) * \mathcal{F}(g(n)) = F(k) * G(k) \tag{3.9}$$

here the $*$ symbol is convolution. And the Fourier transform of a rectangular window is $\text{sinc}(\pi f)$:

$$\int_{-\infty}^{\infty} \text{rect}(t) \cdot e^{-i2\pi ft} = \frac{\sin(\pi f)}{\pi f} = \text{sinc}(\pi f) \tag{3.10}$$

the window function $\text{rect}(t)$ is defined as

$$\text{rect}(t) = \begin{cases} 0 & \text{if } |t| > \frac{1}{2} \\ \frac{1}{2} & \text{if } |t| = \frac{1}{2} \\ 1 & \text{if } |t| < \frac{1}{2} \end{cases} \tag{3.11}$$

The DFT of the N-points series with mapped frequency is

$$|E(f_k)|^2 = \sum_{k=-\infty}^{\infty} |\delta(f_{min} + k\Delta f_{rep} - f_k) * \text{sinc}(f_{min} + k\Delta f_{rep} - f_k)|^2 \tag{3.12}$$

An example of the amplitude spectrum of sinc function is shown in Fig 3.3(b)

Note that in Fig 3.3(b), the sinc function has minimum at integer bin N and peak at $N + 0.5$. This means that if the frequency of the sine wave is at integer bin N, then a Fourier transformed spectrum would have minimized sideband amplitude(We name it "on-grid"); on the other hand, if the sine wave has a frequency of $N + 0.5$, the sideband amplitude is then maximized("off-grid"), as shown in Fig 3.4.

This phenomena is named "spectral leakage" as the sidebands greatly broadens the off-grid sample of the spectrum. Sometimes it's referred as "scalloping loss" for the flattened shape of the peak [35].

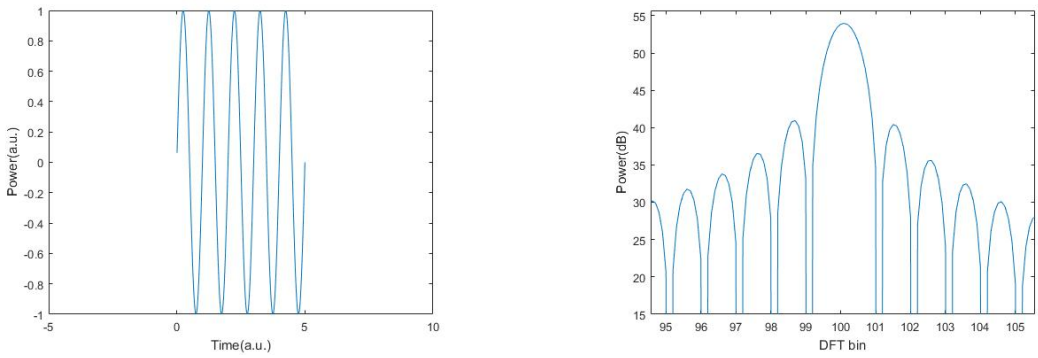

(a) (b)

Fig. 3.3. (a) a sine wave truncated by a rectangular window. (b) DFT of the truncated waveform, showing a sinc function in frequency domain.

In our experiment, the RF spectrum is a sequence of comblines with frequency $f_{min} + k\Delta f_{rep}$. To minimize spectral leakage, the comblines should be close to an integer DFT bin, which means that the spacing between lines Δf_{rep} should equal to some integer multiple of spectral resolution $\frac{f_s}{N}$:

$$\Delta f_{rep} = n \times \frac{f_s}{N}, n \in \mathbb{Z}^+ \tag{3.13}$$

so we could tune the number of points sampled N such that

$$n = \frac{N\Delta f_{rep}}{f_s} \tag{3.14}$$

is a integer. As the time domain envelope also varies at frequency Δf_{rep}, this effectively means that the N that satisfied equation 3.13 in frequency domain also truncated integer multiple of envelope cycles in time domain. The conclusion provides a simple method when selecting suitable N in experiment, which we'll discuss in chapter 4.

Another problem involved by spectral leakage is if n has a small offset from a certain integer, then the actual DFT bin spacing would also be slightly off from Δf_{rep}. Instead of a total leakage, a walk-off of leakage would occur where the extent of leakage ripples throughout the spectrum, as shown in Fig 3.5.

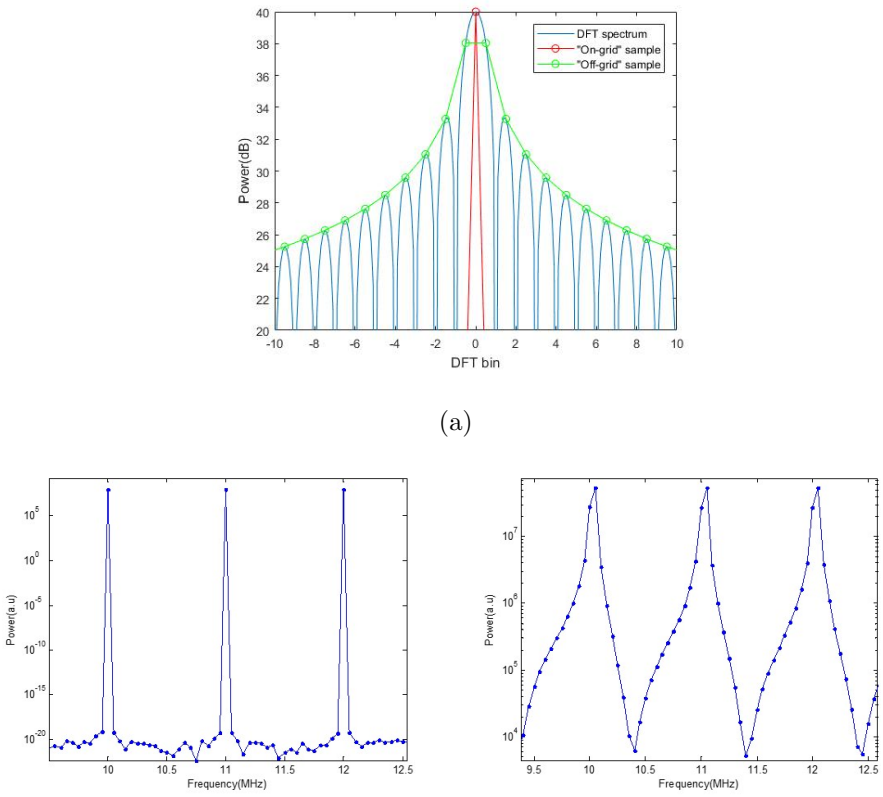

(a)

(b)

(c)

Fig. 3.4. (a)Illustration of a sinc shaped spectrum sampled at N points and at $N + 0.5$ points. (b)An actual example of "on-grid" sample. (c)An actual example of "off-grid" sample

An approach to solve this problem is increasing N to improve spectral resolution $\frac{f_s}{N}$, thus reveal details of the spectrum sidebands to get rid of possible leakage. But due to the stability limitation of the beat signal, N can't be made infinitely large. Thus zero-padding the captured sequence has a effect in revealing sidebands without actually extending the measurment time.

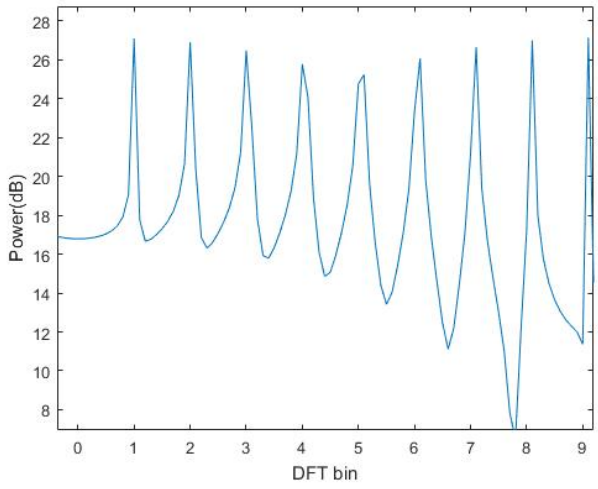

Fig. 3.5. Intensity ripple from spectral leakage.

3.2.3 Time shift

As equation 3.2 shows, the sampled signal can be represented by

$$E(t) = \sum_{k=0}^{n} a_k e^{i(2\pi f_k t + \phi_k)}$$

For the accuracy of measurement, phase result from different time windows are averaged. But when capturing different time windows, a time shift with respect to the envelope is introduced, thus introduced a linear phase shift:

$$\begin{aligned} E(t+\Delta t) = & \sum_{k=0}^{n} a_k e^{i[2\pi f_k (t+\Delta t)+\phi_k]} \\ = & \sum_{k=0}^{n} a_k e^{i[2\pi f_k t+(\phi_k + f_k \Delta t)]} \end{aligned} \tag{3.15}$$

if we apply $f_k = f_{min} + k\Delta f_{rep}$ to equation 3.15

$$E(t+\Delta t) = \sum_{k=0}^{n} a_k e^{i[2\pi f_k t + f_{min}\Delta t + (\phi_k + k\Delta f_{rep}\Delta t)]} \tag{3.16}$$

Thus a linear term $\phi(\Delta f_{rep}) = k\Delta f_{rep}\Delta t + f_{min}\Delta t$ is applied to each ϕ_k. This term should be removed before trying to average phase result from different time windows.

A zero-phase reference is need between different measurements, which method will be discussed in chapter 4.

4. EXPERIMENTAL RESULTS

4.1 Experimental Setup

The experiment setup is shown in Fig 4.1. The beating signal is generated by a 2×2 50/50 coupler for maximum power efficiency. Balanced detector is used for common mode suppression to maximize SNR. The polarization controller in line is used to ensure that reference comb and signal comb have the same polarization, thus maximizing power of the beat signal.

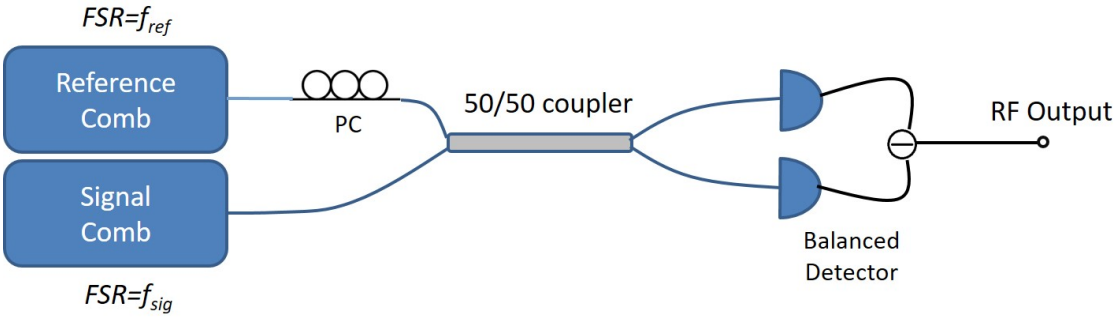

Fig. 4.1. Basic experimental setup. PC, polarization controller.

The RF output is then sampled by a digital oscilloscope. As in our experiments the useful signal has a frequency range of $[0, \frac{f_{ref}}{2}]$, so the f_{ref} signal from the reference comb and signal with frequency higher than $\frac{f_{ref}}{2}$ is suppressed using low-pass RF filters before sampling. Properties of the low-pass filter are listed in Table 4.1. The sampled sequence is then sent to a DFT algorithm for phase retrieval, as shown in Fig 4.2. Properties of the balanced detector and 2×2 coupler is listed in Table 4.2 and Table 4.3.

Fig. 4.2. Digital signal processing(DSP) of the sampled signal

Table 4.1.
Electrical specifications of low-pass filter - Mini-Circuits BLP-150+ / BLP-250+

	BLP-150+	BLP-250+
Passband (loss $<$ 1 dB)	DC-140 MHz	DC-225 MHz
f_{co} (loss = 3 dB)	155 MHz	250 MHz
Stopband (loss $>$ 20 dB)	210-300 MHz	320-400 MHz
Stopband (loss $>$ 40 dB)	300-600 MHz	400-1200 MHz

Table 4.2.
Technical data of balanced detector - Thorlabs PDB460C

Detector Material / Type	InGaAs / Pin
Operate Wavelength	$800 - 1700$ nm
Max. Responsivity	1.0 A/W
RF Output Bandwidth (-3dB)	DC - 200 MHz
CMRR	$>$ 25dB
CW Saturation Power	120μW @ 1550 nm
Overall Output Voltage Noise	2.3 mV_{RMS}

4.1.1 Stability limit

As we discussed in Chapter 3, the sampling time can't be infinitely large due to the instability of the beat signal. Drift in repetition rate and pump laser frequency of

Table 4.3.
Data sheet of 50/50 optical coupler

Operate Wavelength	1550 ± 40nm
Fiber Type	SMF-28e fiber with 900μm loose tube
Splitting Ratio	50:50
Connector	FC/UPC

the combs can cause the beat signal to jitter. A stable measurement can only be made in a time window where jittering of the beat signal is much smaller than the spectral frequency resolution $\frac{f_r}{N}$. An example of multiple peaks in spectrum introduced by longer time window is shown in Fig 4.3.

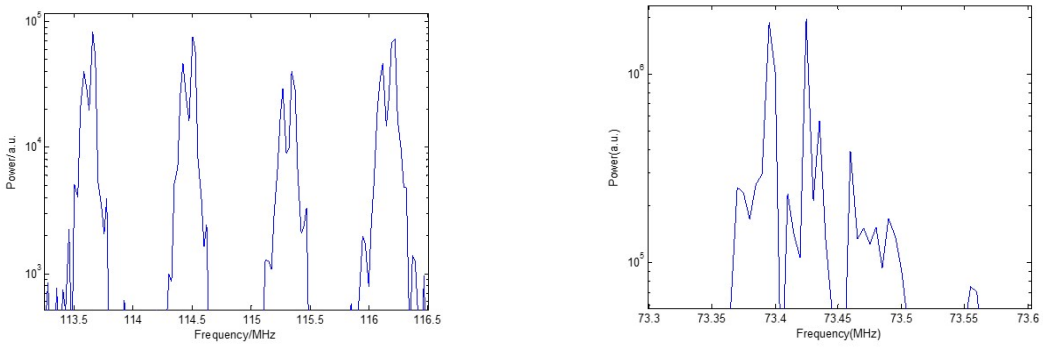

(a) (b)

Fig. 4.3. (a) Dual-peaks appear at 40 μs time window. (b) Multiple peaks due to jittering at 100 μs time window.

Unless otherwise specified, the reference comb we used is a mode-locked laser based optical frequency comb by MenloSystems, with free spectral range $f_{ref} = 250$ MHz. Sampling rate of the oscilloscope is $f_s = 4f_{ref} = 1$ GHz. And a time window used for DFT is ≈ 10 μs ($\approx 10,000$ sampled points). Properties of the reference comb are listed in Table 4.4.

Table 4.4.
Technical data of MenloSystem Comb

Comb spacing	250 MHz
Accuracy	10^{-14} or same as reference
Stability	$5 \cdot 10^{-13}$ in 1 sec. or same as reference
Tuning Range of Spacing	> 2 MHz
Tuning Range of f_{CEO}	≈ 250 MHz
Central Wavelength	1560 nm
Spectral Range	> 35 nm

4.1.2 Phase retrieval algorithm

The phase retrieval algorithm is done through peak detection of the DFT spectrum. To illustrate the phase retrieval process, an example experiment on a Kerr comb ($f_{sig} = 227$ GHz) is performed. The DFT spectrum is shown in Fig 4.4.

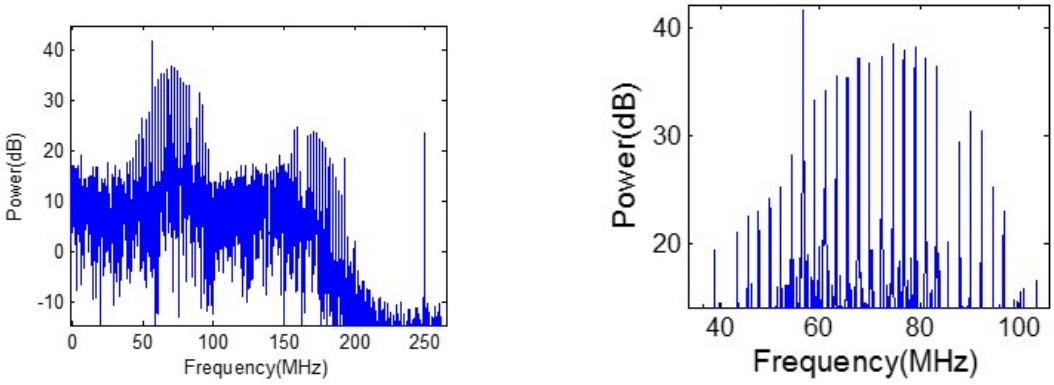

(a) (b)

Fig. 4.4. (a) RF spectrum of beat signal between Menlo reference comb and a Kerr comb. (b) Fig 4.4(a) enlarged to show details of the down-converted spectrum.

Discussions in section 3.2 ensure the spectrum has minimum spectral leakage and only one pixel at each of the peaks. A simple peak detection algorithm would locate the peaks and corresponding phase of each line. Then phase data from different sets are averaged after removing constant and linear phase difference between sets. This is done through the following procedure:

1. Select a certain line as zero-phase reference, often the line with the highest power for stability of the algorithm. The phase difference between the reference line and zero is the constant difference ϕ_c.

2. Subtract the ϕ_c from every set of phases. Then the constant difference is removed.

3. For each phase set, select the next line from the zero-phase reference. The phase difference between the next line and zero is the linear difference for this set ϕ_l.

4. Label each measured line with a index $k_i = i$, where the zero reference selected in step 1 is labeled $k_0 = 0$.

5. Apply a linear phase $-k_i\phi_l$ to each line k_i. Then the linear phase difference is removed.

6. We can repeat step 3 to 5 by selecting a linear reference line N lines away from the zero reference to avoid accumulated error by the linear fit. Note that now the linear coefficient is $\frac{\phi_N}{N}$ instead of ϕ_N.

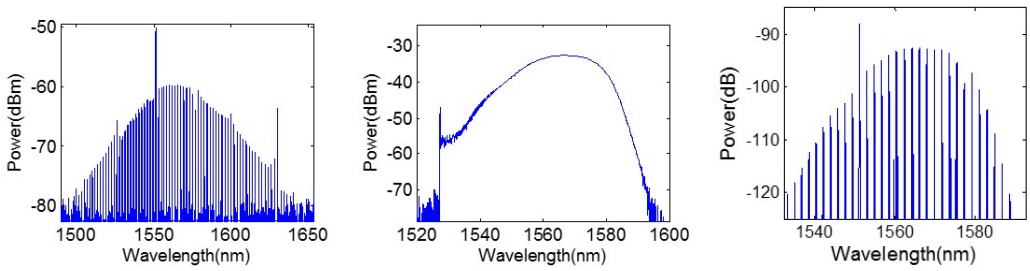

(a) (b) (c)

Fig. 4.5. (a) Spectrum of Kerr comb. (b) Spectrum of the reference comb. (c) Line-by-line product between signal and reference comb

Then the averaged phase of each RF line is applied to the optical combline to show the phase of each line. Fig 4.5 shows the spectrum of signal and reference comb (4.5(a), 4.5(b)), and also the product between the signal and reference comb (4.5(c)). Notice the similarity between Fig 4.4(b) and 4.5(c), giving evidence that the beat signal serves as a down-converted optical spectrum as derived in equation 2.5.

The reference comb is first compressed to near transform-limited to meet the condition of $\phi_{ref} \approx 0$. An example of measured phase with constant and linear difference removed is shown in Fig 4.6. Note the quadratic phase introduced by extra fiber link in the setup. The length of the link is measured and corresponding phase is removed to get actual phase of the comb.

In the example shown in Fig 4.6, the power the signal and reference comb is listed in table 4.5 as a reference for sensitivity limit of the measurement. Actual sensitivity can be improved by using longer time window and larger frequency offset Δf_{rep}, which are limited by the FSR of the reference comb f_{ref} and stability of the beat signal.

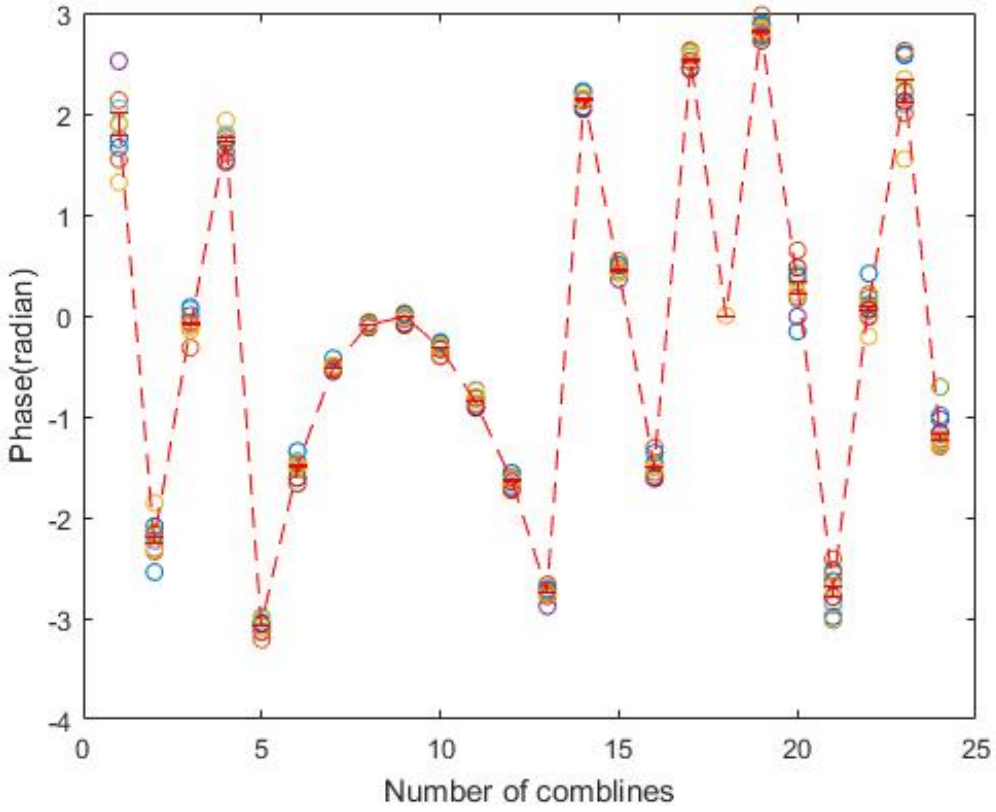

Fig. 4.6. Example of measured phase over 10 different time windows. Average error-bar of the measured phase is 0.02 radian

Table 4.5.
Power limit of measurement in Fig 4.6

	Signal comb	Reference comb
Total power	20 μW	0.5 mW
Average line power	1 μW	15 nW
Minimum line power	250 nW	1.3 nW

4.1.3 Choosing Δf_{rep}

As derived in chapter 2, the offset frequency $\Delta f_{rep} = f_{sig} - n f_{ref}$ represents not only the spacing between lines of RF spectrum, but also the frequency of the

envelope in time domain. For a time window of given length limited by signal stability, larger Δf_{rep} would increase the number of envelope cycles captured, thus increase resolvability of the RF spectrum. But meanwhile, equation 2.11 sets the upper bound for Δf_{rep}. In practical setup, as $f_{ref} = 250$ MHz, $N_{line} \approx 25$, we often choose $\Delta f_{rep} = 3 - 4$ MHz for best result.

4.2 EO-comb phase measurement

Electrooptic comb, EO-comb for short, as discussed in section 1.1.2, has a broadly tunable FSR controlled by the driving RF frequency. It also has a easily tunable f_{ceo} as well as center wavelength controlled by input CW laser frequency.

The basic scheme is shown in Fig 4.7. First measurement measures the phase difference between EO and reference comb $\phi_0 = \phi_{EO} - \phi_{ref}$. Then EO-comb is sent through a pre-characterized component with phase response $\Delta\phi$. The second measurement measures the phase between the reference comb and EO-comb after the medium $\phi_1 = (\phi_{EO} + \Delta\phi) - \phi_{ref}$. Then we compare the two results with the phase response of the component to see whether $\phi_1 - \phi_0 = \Delta\phi$ to test the accuracy of the measurement.

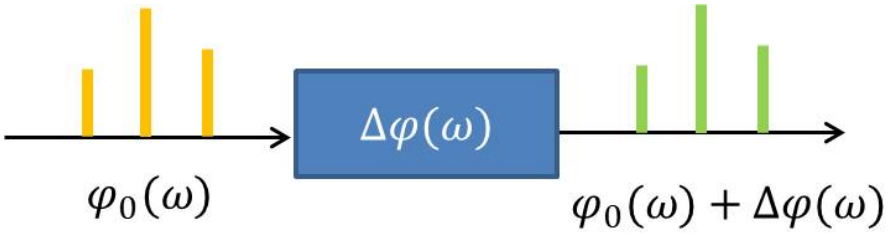

Fig. 4.7. Scheme of phase measurement between EO-comb and reference comb

In this section, the reference comb is the 250 MHz mode-locked laser described in Table 4.4. The signal comb is an EO-comb with ~ 20 lines and repetition rate of 10 GHz.

4.2.1 π shift step function

In this experiment the phase shift component is a conventional pulse shaper based on spatial light modulators [36]. The principle of shaping is shown in Fig 4.8. Different frequency components from the input light are spread and collimated in space by a combination of grating and lens. Then a programmable mask applies different phase on these spatially separated frequencies. And another lens-grating combination reassemble these frequencies to a collimated beam with shifted phase. The specification of the pulse shaper we used is listed in table 4.6.

Table 4.6.
Specification of pulse shaper - Finisar 1000S

Operating Frequency	191.250 THz - 196.275 THz
Operating Wavelength	1527.4 nm - 1567.5 nm
Filter bandwidth	10 GHz - 5 THz
Frequency Setting Resolution	$\pm$1 GHz
Settling Time	500 ms

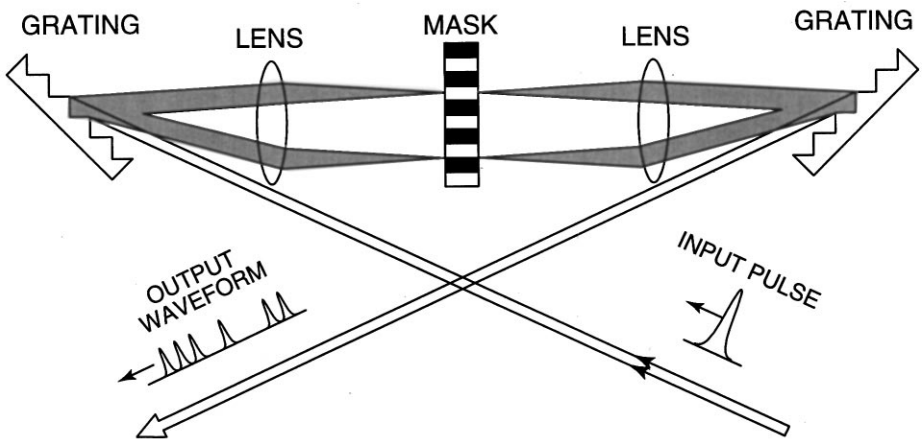

Fig. 4.8. Scheme of pulse shaping [36]

The phase difference we applied is a gate function with height π. The comparison between applied phase $\Delta\phi$ and measured difference $\phi_1 - \phi_0$ is shown in Fig 4.9. The standard variation between different sets of data is less than $5 \cdot 10^{-3}$.

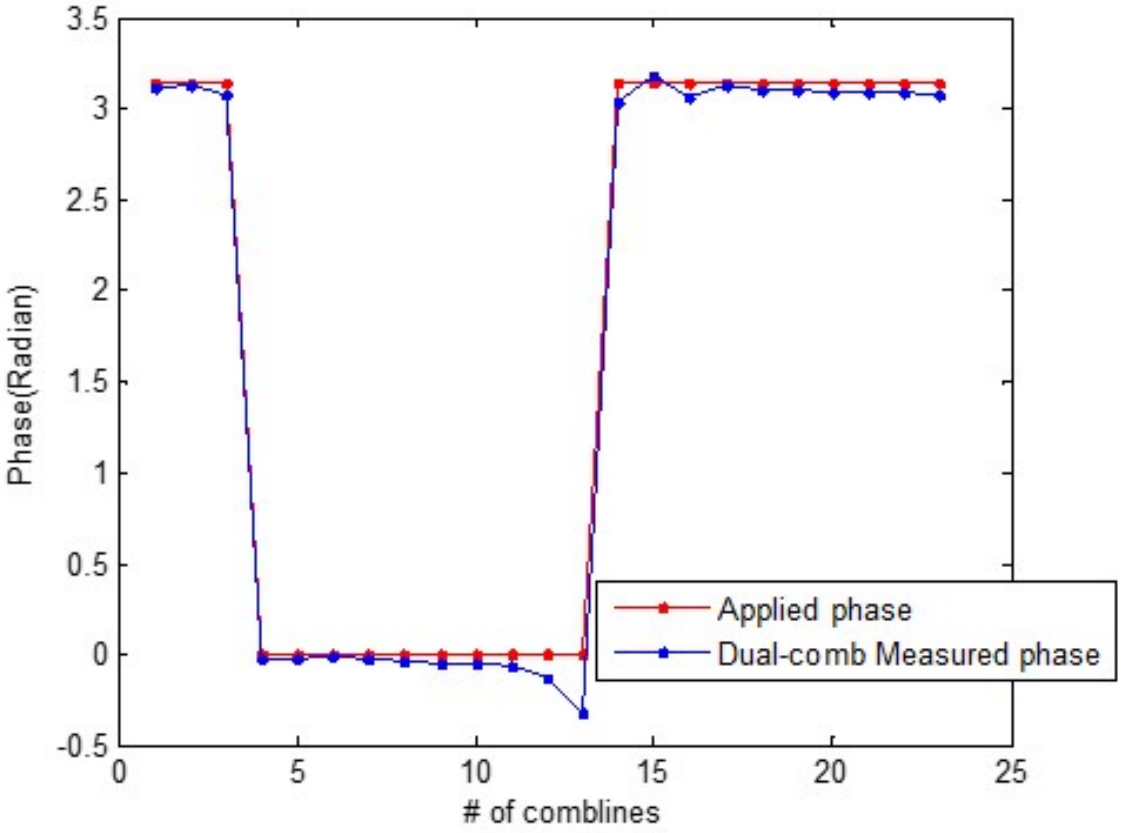

Fig. 4.9. Comparison between dual-comb measured phase and step function applied.

4.2.2 Quadratic phase

Using the same signal and reference comb from section 4.2.1, We apply a quadratic phase with respect to frequency to simulate a single-mode fiber (SMF) link. The pulse shaper described in Table 4.6 has 5025 programmable pixels, each with frequency

$$f(i) = (191.250 + i/1000)\ \text{THz} \tag{4.1}$$

The phase applied on the ith pixel is

$$\phi(i) = 3 \cdot 10^{-5} \times (i - 2012)^2 (\text{radian}) \tag{4.2}$$

thus in frequency, the quadratic phase can be written as

$$\phi(f) = 3 \cdot 10^{-5} \times [\frac{f - f(2012)}{1\ \text{GHz}}]^2 = 3 \cdot 10^{-5} \times [\frac{f - 193.262\ \text{THz}}{1\ \text{GHz}}]^2 \tag{4.3}$$

The comparison between applied and measured phase is shown in Fig 4.10.

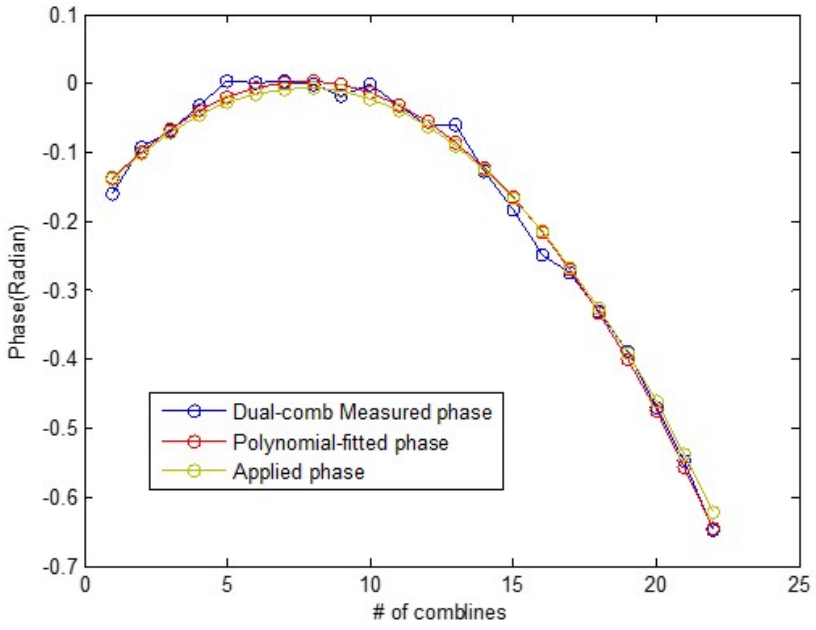

Fig. 4.10. Comparison between dual-comb measured phase and quadratic phase applied. Average error is less than 0.02 radian

.

4.3 Kerr comb phase measurement

With accuracy of the measurement proved in section 4.2, we now apply this method to combs generated through a microresonator. To measure the absolute phase of these combs, a reference with known phase is needed.

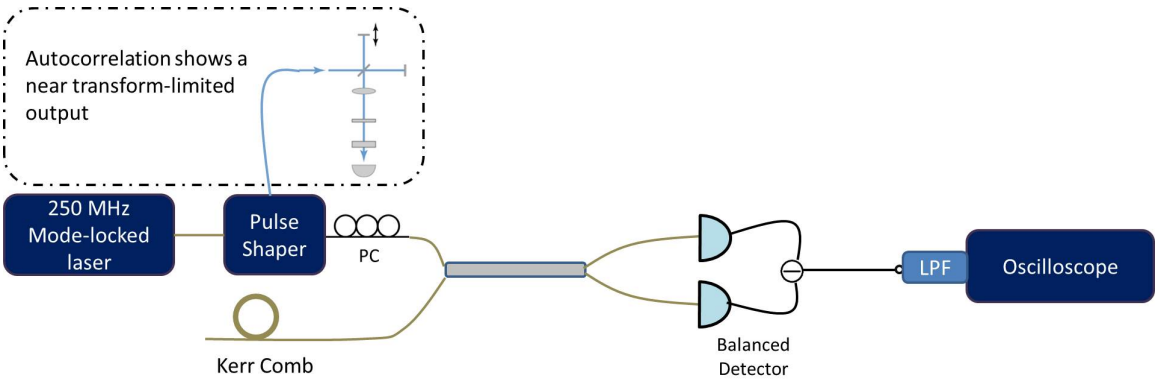

Fig. 4.11. Setup for Kerr-comb phase measurement. PC, polarization controller; LPF, RF low-pass filter

In Fig 4.11, we first characterize the reference comb using a pulse shaper. The output from the pulse shaper is sent into a autocorrelator to measure its autocorrelation trace. Second and third order phase is compensated by the pulse shaper in order to acquire a transform limited pulse from the reference comb. The specification of the pulse shaper used is listed in table 4.7(which is almost twice the bandwidth of listed in table 4.6).

An autocorrelation trace of 250 fs is captured by the autocorrelator, corresponding to a $\sim$ 170 fs pulse assuming a Gaussian shaped pulse. The autocorrelation trace is shown in Fig 4.12. As Fourier transform of the spectrum gives a $\sim$ 150 fs transform-limited pulse. We can say that the 170 fs pulse is capable of serving as a reference with approximately flat phase profile. Then with $\phi_{ref} \approx 0$, the measured phase $\phi_0 = \phi_{sig} - \phi_{ref}$ directly represent the phase from the signal comb.

Table 4.7.
Specification of pulse shaper - Finisar 4000S

Operating Frequency	187.275 THz - 196.275 THz
Operating Wavelength	1527.4 nm - 1600.8 nm
Filter bandwidth	20 GHz - 9 THz
Frequency Setting Resolution	±1 GHz
Settling Time	500 ms

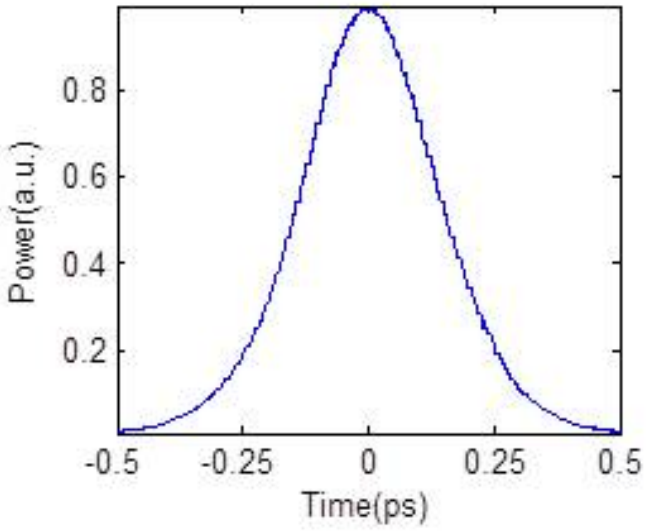

Fig. 4.12. Autocorrelation trace of the reference comb. FWHM is 250 fs

4.3.1 Single soliton comb

Following the setup in Fig 4.11, we measured the phase of a Kerr comb in single soliton regime. The microring is the same with the one reported in [37] with quality factor Q $\approx 3 \times 10^6$, FSR = 228 GHz and dispersion $\beta_2 = -61$ ps^{2}km^{-1}. As shown in Fig 4.13, the phase profile consists of a flat background and a phase offset at pump line.

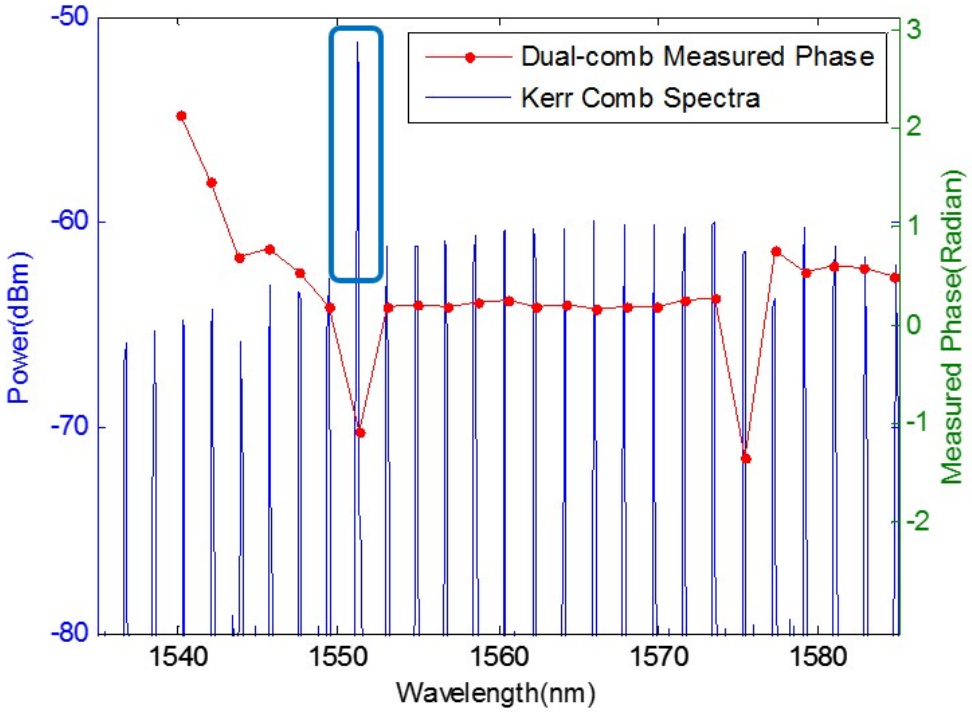

Fig. 4.13. Measured phase of a single soliton comb. The circled line is the pump line of the comb. The measured phase profile shows a phase offset of $\sim$ -1.5 radian from the flat background.

The measured phase have a bandwidth from 1540 nm to 1580 nm, which is limited by the bandwidth of the reference comb we can generate using a pulse shaper. The rising tail at $\sim$1545 nm might come from higher order phase term of the reference comb.

Pump line phase offset is defined as the phase offset between pump line phase and the flat soliton phase background. This offset has been a interesting topic in Kerr comb researches as the offset describes the interference between CW background and soliton phase [38]. As we further detune the pump laser, the phase offset of the pump line changes with detuning as well, shown in Fig 4.14(b)

Earlier line-by-line measurement and simulation [37,38] shows possible offset from $-\pi/3$ to -0.42 rad, as shown in Fig 4.15. Our dual-comb measurement acquired offset phase from -1.54 rads to -0.4 rad, showing broader possible range.

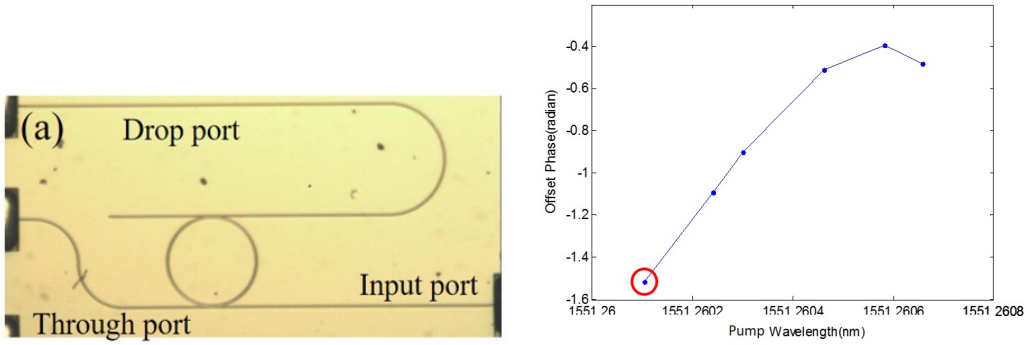

(a) (b)

Fig. 4.14. (a) Microresonator used to generate single soliton comb. [37] (b) Change of pump line phase offset with respect to pump wavelength. The circled point is the case measured in Fig 4.13.

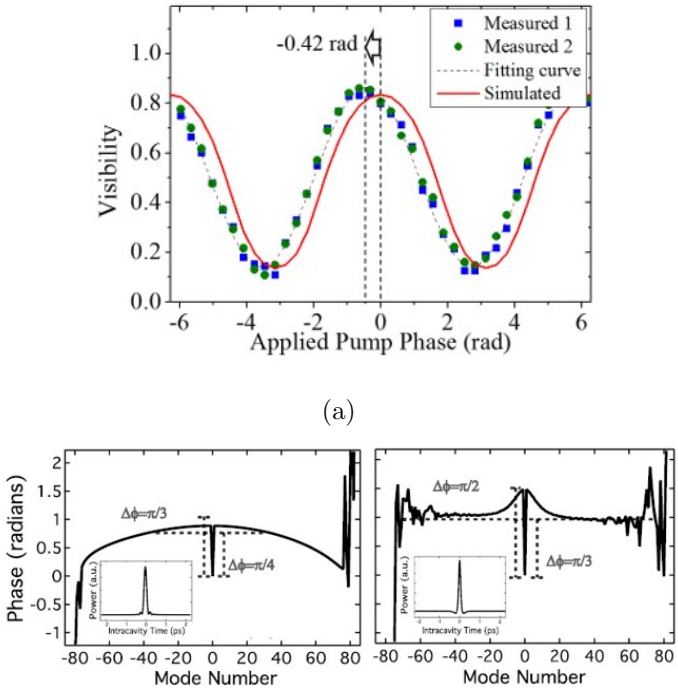

(a)

(b)

Fig. 4.15. (a) -0.42 rad offset phase measured by line-by-line phase shaping [37] (b) $-\pi/3$ to $-\pi/4$ offset predicted by simulation from LL-equation [38].

4.3.2 Dark soliton comb

Repeating the experiment on a SiN microring demonstrated in [39]. The ring has a a normal dispersion $\beta_2 = 190.7 \pm 8.4$ ps^{2}km^{-1} with loaded quality factor Q $\approx 7.7 \times 10^5$ and FSR = 231.3 GHz. The measured phase is shown in Fig 4.16. As seen from Fig 4.16(b), phase retrieved by dual-comb measurement matches closely to result from line-by-line shaping.

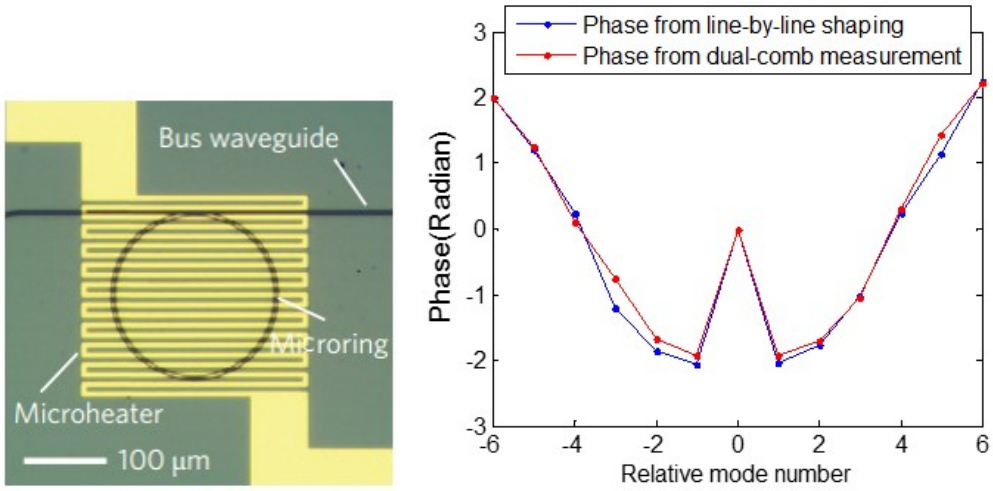

(a) (b)

Fig. 4.16. (a) Structure of the microresonator for dark soliton generation. (b) Comparison between phase measured by dual-comb and by line-by-line shaping [39].

4.3.3 Multiple soliton comb

Using the same setup in Fig 4.11, phase from a multiple soliton comb is also measured. An inverse Fourier transform using measured phase and spectrum from OSA gives the time domain trace of the multi-soliton comb, shown in Fig 4.17.

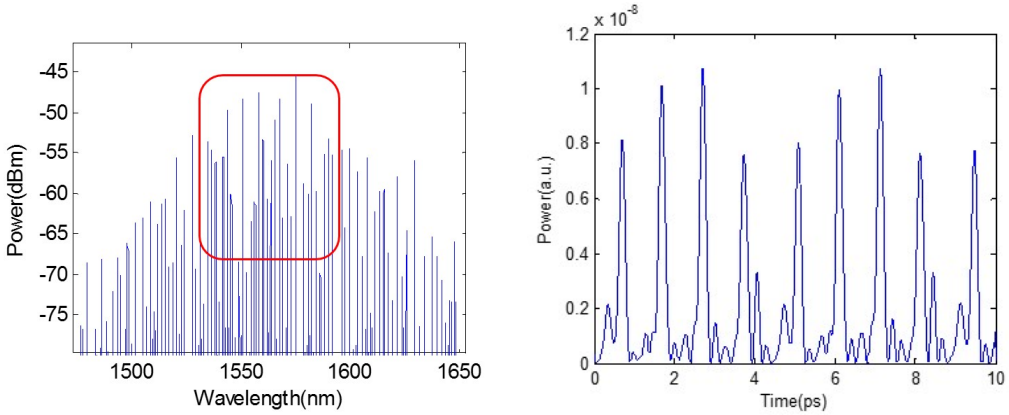

(a) (b)

Fig. 4.17. (a) Spectrum of multiple soliton comb. The lines circled are the lines with measured phase. (b) Retrieved time trace using measured phase data, showing 4 solitons in a round trip cycle.

The circled lines in Fig 4.17(a) consists about 80% of the comb energy. As we increase the number of lines involved in reverse Fourier transform, the relative position between solitons stays the same but no solid conclusion can be made towards the relationship between the amplitude and pulse-width of the solitons are identical or not as unmeasured lines can still affect soliton power. The evolution of time trace with change in line number is shown in Fig 4.18.

In order to have an estimation of the bandwidth needed to predict if the solitons are of identical amplitude, we perform a numerical simulation using MATLAB. In this simulation, we construct a optical spectrum corresponding to a time-domain trace of 4 solitons per round trip with equal amplitude. As we already knew the phase of each line in the simulation, we can gradually reduce the number of lines involved in the field reconstruction process to see whether the retrieved pulses are still of equal

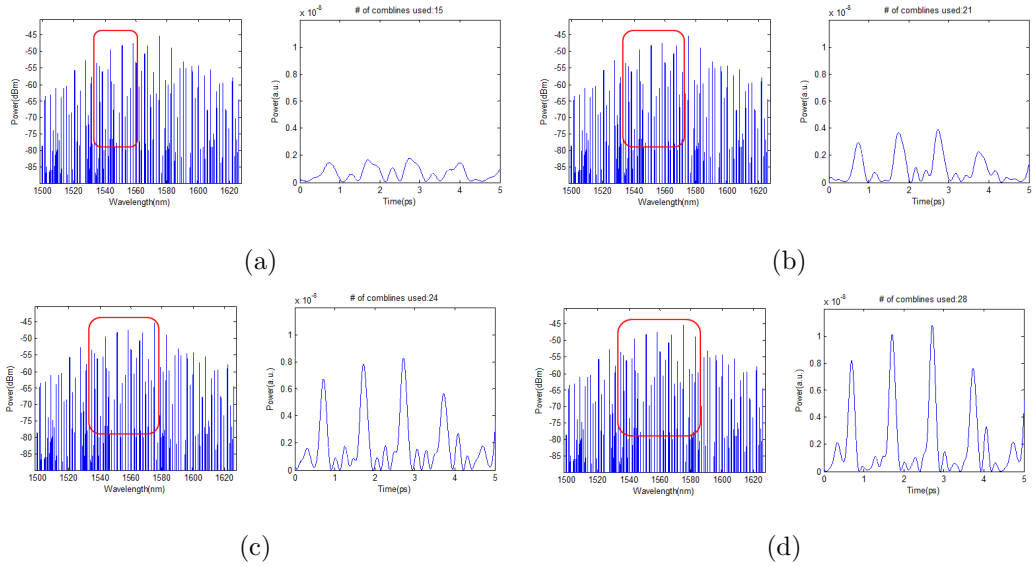

Fig. 4.18. The evolution of retrieved time trace using phase from circled (a) 15 lines; (b) 21 lines; (c) 24 lines; (d) 28 lines, showing relative position of each soliton

amplitude, as shown in Fig 4.19. The actual bandwidth requirement may differ from different input spectrum, but typically for a power difference tolerance of 5%, the result from the simulation shows that a measurement covering $\sim$ 8 THz bandwidth or 90% of the total power is needed.

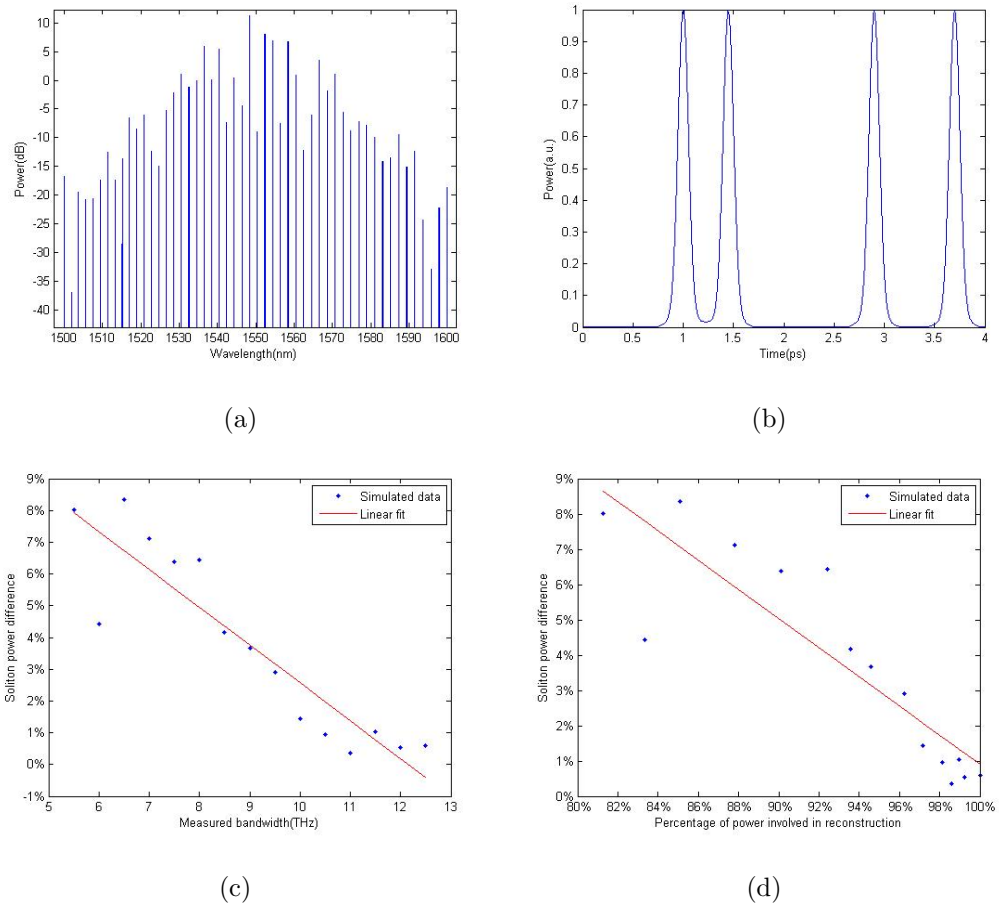

(a) (b)

(c) (d)

Fig. 4.19. Simulation of bandwidth requirement of multiple soliton field reconstruction (a) Example spectrum used in simulation; (b) Reconstructed time-domain trace; (c) Change in retrieved soliton amplitude with respect to simulation bandwidth; (d) Change in retrieved soliton amplitude with respect to covered power of input comb

5. SUMMARY

In this thesis, we demonstrated a phase measurement method based on dual-comb electric field cross-correlation(EFXC). This method provides a way towards full characterization of optical frequency combs without nonlinear process, thus it greatly lowers the power requirement compared to conventional methods like frequency-resolved optical gating(FROG). With a pre-characterized reference comb, optical phase of signal comb can be retrieved by simply measuring the phase of beat RF signal between combs, and experimental results shows a measurement precision of ~ 0.02 rad.

Using this method, phase data from a single soliton comb and dark soliton comb are measured and matches closely to theoretical prediction or result from conventional line-by-line shaping. Phase data from multiple soliton comb reveals the time trace and relative position between multiple solitons. The phase response of a unknown optical component can also be measured by using two comparative measurements.

Future works on dual-comb phase measurement will focus on pushing the limit of this method. E.g. creating reference comb with broader spectrum would greatly increase bandwidth limit of the measurement; removing higher order phase term from reference would eliminate unexpected 'tails' in retrieved phase. Using reference with higher FSR would rise the upper bound of offset frequency Δf, thus more envelope cycles can be captured in the same time window, increasing stability of the measurement. Applying this method to measurement of multi-mode fiber phase response also has great potential in optical communications.

Due to the low power requirement of this method, it can be applied to low-power, high duty cycle devices which phase has yet to be measured due to the limitation of output power, thus a new way of optical waveform characterization has been discovered, and revealed exciting opportunities for further exploration of optical frequency combs.

REFERENCES

REFERENCES

[1] R. Trebino and D. J. Kane, "Using phase retrieval to measure the intensity and phase of ultrashort pulses: frequency-resolved optical gating," *JOSA A*, vol. 10, no. 5, pp. 1101–1111, 1993.

[2] C. Iaconis and I. A. Walmsley, "Spectral phase interferometry for direct electric-field reconstruction of ultrashort optical pulses," *Optics letters*, vol. 23, no. 10, pp. 792–794, 1998.

[3] I. Coddington, W. C. Swann, and N. R. Newbury, "Coherent multiheterodyne spectroscopy using stabilized optical frequency combs," *Physical Review Letters*, vol. 100, no. 1, p. 013902, 2008.

[4] F. Ferdous, D. E. Leaird, C.-B. Huang, and A. Weiner, "Dual-comb electric-field cross-correlation technique for optical arbitrary waveform characterization," *Optics letters*, vol. 34, no. 24, pp. 3875–3877, 2009.

[5] R. Fork, B. Greene, and C. V. Shank, "Generation of optical pulses shorter than 0.1 psec by colliding pulse mode locking," *Applied Physics Letters*, vol. 38, no. 9, pp. 671–672, 1981.

[6] S. T. Cundiff and J. Ye, "Colloquium: Femtosecond optical frequency combs," *Reviews of Modern Physics*, vol. 75, no. 1, p. 325, 2003.

[7] S. Hadjiloucas, G. Walker, J. Bowen, V. Becerra, A. Zafiropoulos, and R. Galvão, "High signal to noise ratio thz spectroscopy with asops and signal processing schemes for mapping and controlling molecular and bulk relaxation processes," in *Journal of Physics: Conference Series*, vol. 183, no. 1. IOP Publishing, 2009, p. 012003.

[8] K. Minoshima and H. Matsumoto, "High-accuracy measurement of 240-m distance in an optical tunnel by use of a compact femtosecond laser," *Applied Optics*, vol. 39, no. 30, pp. 5512–5517, 2000.

[9] J. L. Hall, "Defining and measuring optical frequencies: the optical clock opportunityand more (nobel lecture)," *ChemPhysChem*, vol. 7, no. 11, pp. 2242–2258, 2006.

[10] D. Nicolodi, B. Argence, W. Zhang, R. Le Targat, G. Santarelli, and Y. Le Coq, "Spectral purity transfer between optical wavelengths at the 10-18 level," *Nature Photonics*, vol. 8, no. 3, pp. 219–223, 2014.

[11] Nobelprize.org, *The Nobel Prize in Physics 2005*, 2005 (accessed March 1, 2016). [Online]. Available: http://www.nobelprize.org/nobel_prizes/physics/laureates/2005

[12] T. Udem, J. Reichert, R. Holzwarth, and T. Hänsch, "Absolute optical frequency measurement of the cesium d 1 line with a mode-locked laser," *Physical review letters*, vol. 82, no. 18, p. 3568, 1999.

[13] H. R. Telle, G. Steinmeyer, A. Dunlop, J. Stenger, D. Sutter, and U. Keller, "Carrier-envelope offset phase control: A novel concept for absolute optical frequency measurement and ultrashort pulse generation," *Applied Physics B: Lasers and Optics*, vol. 69, no. 4, pp. 327–332, 1999.

[14] Y.-J. Kim, I. Coddington, W. C. Swann, N. R. Newbury, J. Lee, S. Kim, and S.-W. Kim, "Time-domain stabilization of carrier-envelope phase in femtosecond light pulses," *Optics express*, vol. 22, no. 10, pp. 11 788–11 796, 2014.

[15] P. Pal, W. H. Knox, I. Hartl, and M. E. Fermann, "Self referenced yb-fiber-laser frequency comb using a dispersion micromanaged tapered holey fiber," *Optics express*, vol. 15, no. 19, pp. 12 161–12 166, 2007.

[16] A. Cingöz, D. Yost, T. Allison, A. Ruehl, M. Fermann, I. Hartl, and J. Ye, "Broadband phase noise suppression in a yb-fiber frequency comb," *Optics letters*, vol. 36, no. 5, pp. 743–745, 2011.

[17] C. Li, Y. Ma, X. Gao, F. Niu, T. Jiang, A. Wang, and Z. Zhang, "1 ghz repetition rate femtosecond yb: fiber laser for direct generation of carrier-envelope offset frequency," *Applied optics*, vol. 54, no. 28, pp. 8350–8353, 2015.

[18] M. Hofer, M. E. Fermann, F. Haberl, M. Ober, and A. Schmidt, "Mode locking with cross-phase and self-phase modulation," *Optics letters*, vol. 16, no. 7, pp. 502–504, 1991.

[19] H. Haus, K. Tamura, L. Nelson, and E. Ippen, "Stretched-pulse additive pulse mode-locking in fiber ring lasers: theory and experiment," *IEEE Journal of quantum electronics*, vol. 31, no. 3, pp. 591–598, 1995.

[20] D. J. Jones, S. A. Diddams, J. K. Ranka, A. Stentz, R. S. Windeler, J. L. Hall, and S. T. Cundiff, "Carrier-envelope phase control of femtosecond mode-locked lasers and direct optical frequency synthesis," *Science*, vol. 288, no. 5466, pp. 635–639, 2000.

[21] M. Zimmermann, C. Gohle, R. Holzwarth, T. Udem, and T. W. Hänsch, "Optical clockwork with an offset-free difference-frequency comb: accuracy of sum-and difference-frequency generation," *Optics letters*, vol. 29, no. 3, pp. 310–312, 2004.

[22] T. Nakamura, I. Ito, and Y. Kobayashi, "Offset-free broadband yb: fiber optical frequency comb for optical clocks," *Optics express*, vol. 23, no. 15, pp. 19 376–19 381, 2015.

[23] Q. Cao, Y. Liu, C. Li, X. Gao, Z. Zhang, F. X. Kärtner, and G. Chang, "Passively offset-free yb: Fiber laser source with 1 ghz repetition rate," in *CLEO: Applications and Technology*. Optical Society of America, 2016, pp. JTh2A–141.

[24] Y. Ma, L. Zuo, F. Meng, C. Li, T. Jiang, A. Wang, F. Zhao, G. Zhao, and Z. Zhang, "A compact 30 ghz spaced astro-comb based on 1 ghz yb: fiber laser," in *Lasers and Electro-Optics (CLEO), 2016 Conference on*. IEEE, 2016, pp. 1–2.

[25] H. Murata, A. Morimoto, T. Kobayashi, and S. Yamamoto, "Optical pulse generation by electrooptic-modulation method and its application to integrated ultrashort pulse generators," *IEEE Journal of Selected Topics in Quantum Electronics*, vol. 6, no. 6, pp. 1325–1331, 2000.

[26] A. Yariv, *Quantum Electronics*. Wiley, 1967.

[27] A. M. Weiner, *Ultrafast Optics*. Wiley, 2009.

[28] A. Metcalf, F. Quinlan, T. Fortier, S. Diddams, and A. Weiner, "Broadly tunable, low timing jitter, high repetition rate optoelectronic comb generator," *Electronics letters*, vol. 51, no. 20, pp. 1596–1598, 2015.

[29] P. DelHaye, A. Schliesser, O. Arcizet, T. Wilken, R. Holzwarth, and T. Kippenberg, "Optical frequency comb generation from a monolithic microresonator," *Nature*, vol. 450, no. 7173, pp. 1214–1217, 2007.

[30] T. J. Kippenberg, R. Holzwarth, and S. Diddams, "Microresonator-based optical frequency combs," *Science*, vol. 332, no. 6029, pp. 555–559, 2011.

[31] P. DelHaye, T. Herr, E. Gavartin, M. Gorodetsky, R. Holzwarth, and T. J. Kippenberg, "Octave spanning tunable frequency comb from a microresonator," *Physical Review Letters*, vol. 107, no. 6, p. 063901, 2011.

[32] P. Del'Haye, A. Coillet, T. Fortier, K. Beha, D. C. Cole, K. Y. Yang, H. Lee, K. J. Vahala, S. B. Papp, and S. A. Diddams, "Phase-coherent microwave-to-optical link with a self-referenced microcomb," *Nature Photonics*, vol. 10, no. 8, pp. 516–520, 2016.

[33] K. Naganuma, K. Mogi, and H. Yamada, "Group-delay measurement using the fourier transform of an interferometric cross correlation generated by white light," *Optics letters*, vol. 15, no. 7, pp. 393–395, 1990.

[34] C. E. Shannon, "Communication in the presence of noise," *Proceedings of the IRE*, vol. 37, no. 1, pp. 10–21, 1949.

[35] R. Lyons, "Reducing fft scalloping loss errors without multiplication," *IEEE Signal Processing Magazine*, vol. 28, no. 2, pp. 112–116, 2011.

[36] A. M. Weiner, "Femtosecond pulse shaping using spatial light modulators," *Review of scientific instruments*, vol. 71, no. 5, pp. 1929–1960, 2000.

[37] P.-H. Wang, J. A. Jaramillo-Villegas, Y. Xuan, X. Xue, C. Bao, D. E. Leaird, M. Qi, and A. M. Weiner, "Intracavity characterization of micro-comb generation in the single-soliton regime," *Optics express*, vol. 24, no. 10, pp. 10 890–10 897, 2016.

[38] Y. H. Wen, M. R. Lamont, S. H. Strogatz, and A. L. Gaeta, "Self-organization in kerr-cavity-soliton formation in parametric frequency combs," *Physical Review A*, vol. 94, no. 6, p. 063843, 2016.

[39] X. Xue, Y. Xuan, Y. Liu, P.-H. Wang, S. Chen, J. Wang, D. E. Leaird, M. Qi, and A. M. Weiner, "Mode-locked dark pulse kerr combs in normal-dispersion microresonators," *Nature Photonics*, vol. 9, no. 9, pp. 594–600, 2015.